Title
Analysis of Neural Activity in Human Motor Cortex - towards Brain Machine Interface System

Author
Secundo, Lavi

Publication Date
2010

Peer reviewed|Thesis/dissertation

Analysis of Neural Activity in Human Motor Cortex – towards Brain Machine Interface System

by

Lavi Secundo

A dissertation submitted in partial satisfaction
of the requirements for the degree of

Doctor of Philosophy

in

Neuroscience

in the

GRADUATE DIVISION

of the

UNIVERSITY OF CALIFORNIA, BERKELEY

Committee in charge:

Professor Robert T. Knight, Chair
Professor Richard B. Ivry
Professor Jose M. Carmena
Professor Steve L. Lehman

Spring 2010

Analysis of Neural Activity in Human Motor Cortex – towards Brain Machine Interface System

By

Lavi Secundo

Abstract

Analysis of Neural Activity in Human Motor Cortex – towards Brain Machine Interface System
by
Lavi Secundo

Doctor of Philosophy in Neuroscience
University of California, Berkeley

Professor Robert T. Knight, Chair

The discovery of directional tuned neurons in the primary motor cortex has advanced motor research in several domains. For instance, in the area of brain machine interface (BMI), researchers have exploited the robust characteristic of tuned motor neurons to allow monkeys to learn control of various machines. In the first chapter of this work we examine whether this phenomena can be observed using the less invasive method of recording electrocorticographic signals (ECoG) from the surface of a human's brain. Our findings reveal that individual ECoG channels contain complex movement information about the neuronal population. While some ECoG channels are tuned to hand movement direction (direction specific channels), others are associated to movement but do not contain information regarding movement direction (non-direction specific channels). More specifically, directionality can vary temporally and by frequency within one channel. In addition, a handful of channels contain no significant information regarding movement at all. These findings strongly suggest that directional and non-directional regions of cortex can be identified with ECoG and provide solutions to decoding movement at the signal resolution provided by ECoG.

In the second chapter we examine the influence of movement context on movement reconstruction accuracy. We recorded neuronal signals recorded from electro-corticography (ECoG) during performance of cued- and self-initiated movements. ECoG signals were used to train a reconstruction algorithm to reconstruct continuous hand movement. We found that both cued- and self-initiated movements could be reconstructed with similar accuracy from the ECoG data. However, while an algorithm trained on the cued task could reconstruct performance on a subsequent cued trial, it failed to reconstruct self-initiated arm movement. The same task-specificity was observed when the algorithm was trained with self-initiated movement data and tested on the cued task. Thus, the correlation of ECoG activity to kinematic parameters of arm movement is context-dependent, an important constraint to consider in future development of BMI systems.

The third chapter delves into a fundamental organizational principle of the primate motor system - cortical control of contralateral limb movements. However, ipsilateral motor areas also appear to play a role in the control of ipsilateral limb movements. Several studies in monkeys have shown that individual neurons in ipsilateral primary motor cortex (M1) may represent, on average, the direction of movements of the ipsilateral arm. Given the increasing body of evidence demonstrating that neural ensembles can reliably represent information with a high temporal resolution, here we characterize the

distributed neural representation of ipsilateral upper limb kinematics in both monkey and man. In two macaque monkeys trained to perform center-out reaching movements, we found that the ensemble spiking activity in M1 could continuously represent ipsilateral limb position. We also recorded cortical field potentials from three human subjects and also consistently found evidence of a neural representation for ipsilateral movement parameters. Together, our results demonstrate the presence of a high-fidelity neural representation for ipsilateral movement and illustrates that it can be successfully incorporated into a brain-machine interface.

Acknowledgements

This was not an easy journey and this work could not have been completed without the help mentoring and support of many wonderful people whom I met along the way.

My deepest gratitude is to my advisor, Professor Robert Knight. I have been amazingly fortunate to have an advisor who gave me the freedom to explore on my own and at the same time provide me with the means and guidance to perform my research. Bob taught me how to ask questions and express ideas. His tolerance, open-mindedness and support helped me overcome many crisis situations and finish this dissertation. I hope to continue and collaborate with Bob in the years to come.

My co-advisor Professor Richard Ivry, has been always there to listen and give advice. I am deeply grateful to him for the long discussions that helped me design better experiments, for his insightful comments and constructive criticisms at different stages of my research that were thought-provoking and helped me focus my ideas. I am also thankful to him for carefully reading and commenting on countless revisions of this manuscript.

Professor Jose Carmena who was both a mentor and a close friend. I am grateful to him for introducing me to the field of Brain Machine Interface; his work inspired me on this dissertation. As my first advisor at Berkeley Jose held me to a high research standard and helped me to sort out the technical details of my work thus enabling a lot of this research.

Professor Steve Lehamn is one of the best teachers that I have had in my life. He sets high standards for his students and encourages and guides them to meet those standards. He totally changed my experience as a GSI when I worked for him in the motor control lab. I am indebted to him for his continuous encouragement and guidance. I am also thankful to him for reading my reports; commenting on my views and helping me understand and enrich my ideas.

To Connie Cheung my wonderful research-assistant.

To Professor Noam Sobel, Dr. Ayelet Landau and Amir Angle that initiated all this.

Many friends have helped me stay sane through these difficult years as a foreigner student in the US. Their support and care helped me overcome setbacks and made me feel very much at home. I greatly value their friendship and I will deeply miss them.

Special thanks to Steve Kineerly, Sarah Gillet, Avgusta Shestyuk, Adeen flinker, Charles Cadieu, and Beth Mormino for sharing their lives with me.

Most importantly, none of this would have been possible without the love and patience of my Mom, Dad, Hagar and Maya. My immediate family, to whom this dissertation is dedicated to, has been a constant source of love, concern, support and strength all these years. I would like to express my heart-felt gratitude to my family that has aided and encouraged me throughout this endeavor.

Finally, I appreciate the financial support from UCBREP that funded parts of the research discussed in this dissertation.

Table of Contents

1 Introduction 1

2 Complex directional tuning properties as revealed by human subdural recordings 4

2.1 Background 4

2.2 Methods 5

2.2.1 Data Recordings 5

2.2.2 Behavioral task 6

2.2.3 Analysis 7

2.2.4 Preprocessing 7

2.2.5 Time frequency decomposition 7

2.2.6 Electrodes classification 8

2.3 Results 8

2.3.1 Movement Related spectrograms (non dir tuned) 9

2.3.2 Directional Tuning curves 11

2.3.3 Spectral specificity of directional tuning curves 13

2.3.4 Preferred directions distributions in different spectral frequency bands for a single electrode 14

2.4 Discussion 16

2.4.1 Relation between the high-frequencies, low frequencies and movement: 18

3 Representation of arm kinematics in human cortex is context specific 20

3.1 Background 20

3.2 Methods 21

3.2.1 Data Recordings 22

3.2.2 Behavioral task 22

3.2.3 Analysis 23

3.2.4 Preprocessing 24

3.2.5 Wiener Filter 24

3.2.6 Statistical Analysis 25

3.3 Results 27

3.3.1 Decoding accuracy within context 27

3.3.2 Generalization to a novel context 29
3.3.3 Control analysis of generalization assessment 31
3.4 Discussion 32
3.4.1 Specificity of movement training weights 33
3.4.2 Potential biases 34
3.4.3 Conclusion 36
4 Cortical Representation of Ipsilateral Arm Movements in Monkey and Man 37
4.1 Background 37
4.2 Methods 38
4.2.1 Monkeys 38
4.2.2 Data analysis 40
4.2.3 Human Subjects 41
4.3 Results 43
4.3.1 Monkeys 43
4.3.2 Human Subjects 47
4.3.3 Ipsilateral Neural Representation for closed-Loop BMI in Monkeys 48
4.4 Discussion 49
4.4.1 Conclusion 52
5 Appendix I : Supplementary Figures 53
6 Appendix II: MATLAB codes 59
6.1 ERP - The full algorithm 59
6.2 ERSP - The full algorithm 59
7 References 60

1 Introduction

Every year, severe spinal cord injuries alone are responsible for the occurrence of nearly 11,000 new cases of permanent paralysis in the US. These cases add to an already sizeable population of patients, estimated at 250,000 people in the US who cope with varying degrees of partial or almost total body paralysis. It is hoped that in the near future Brain-Machine Interfaces (BMIs) will have a strong impact on society, especially on the quality of life of people with various degrees of disabilities. This research seeks to advance our understanding of the ways the cortex control upper limb movement and to find ways to utilize this information in the context of BMI, because of this specific focus I will use here the term BMI as the capability to control robots or graphical cursors in real-time through signals obtained from the brain without overt arm movement. The long term goal is to create a brain-controlled prosthesis capable of reproducing the wide range of motor and sensory functions carried out by the human upper limb. And to enable amputees and patients with various nerve impairments to use artificial limbs as natural ones.

It is assumed that there is a compromise between the level of invasiveness and the accuracy of controlling the artificial device using the BMI. By implanting multi-electrode arrays in various sites of a macaque monkey cortex Velliste et al. 2008 (Velliste et al., 2008) have demonstrated the most accurate control so far. The researchers enabled the monkey to feed itself and perform basic reach and grasp movement through BMI without the use of the animal's own limb. A similar setup performed on a quadriplegic human patient enabled the patient to open simulated e-mail, operated devices such as a television using a 'neural cursor' and perform rudimentary actions with a multi-jointed robotic arm. In addition, several researches have demonstrated that information regarding arm movement can be extracted from LFP (Pistohl et al., 2008; Waldert et al., 2009), ECoG (Leuthardt et al., 2004; Leuthardt et al., 2006; Schalk et al., 2008), and EEG (Wolpaw et al., 2002; McFarland et al., 2006) signals and those less invasive methods might be a better choice for the use of BMI as a clinical tool. However, LFP, ECoG, and EEG suffer from a lower SNR compared to single-spike recording and it is still debatable if information required controlling a complex prosthetic device is present in those signals.

In this work I propose that ECoG might an optimal choice for BMI. First, the use of ECoG technique enables recording from multiple neurons and from multiple areas of the brain simultaneously and to study the correlated behavior between ensembles of neurons in different regions of the brain. Second, as our movement reconstruction results detest the ECoG signal is a good compromise between signal quality and invasiveness. This is achieved due to the placement of electrodes directly on the surface of the cortex.

One of the main questions still needed to be answered is the characteristics of the control signal for BMI. While it is known that the cortex plays a critical role in the

production of complex movements, it is still debatable how motor commands, and which motor commands are represented in different parts of the motor cortex. In this work I examine these two questions from three perspectives. First, since directional tuning is one of the corner-stones in movement related activity research in primates' cortex, I examine whether directional tuning information persists in the level of ECoG signals. Second I examine the influence of movement context on the ability to reconstruct hand position and velocity from ECoG signal. And finally I examine the ability to use ipsilateral cortex to decode hand movements.

1. ECOG directional tuning: Despite extensive experimental efforts, recording and stimulating primarily from the arm area of motor cortex, it still remains controversial whether motor cortex encodes specific dynamic features such as the force/torque applied by the hand/joint (Evarts, 1968; Cheney and Fetz, 1980; Taira et al., 1996), kinematic features such as position, velocity, and direction of the limb (Georgopoulos et al., 1982; Georgopoulos et al., 1986; Georgopoulos et al., 1989; Moran and Schwartz, 1999; Paninski et al., 2004a; Paninski et al., 2004b), muscle synergies (Bizzi et al., 2000; Bizzi et al., 2002; d'Avella et al., 2003; d'Avella and Bizzi, 2005), or behaviorally relevant gestures (Graziano et al., 2005; Aflalo and Graziano, 2006; Graziano, 2006; Aflalo and Graziano, 2007). Different behavioral paradigms and various experiments have supported all views. Answering this debate is crucial in understanding how the brain generates the large movement repertoire performed by the primate upper limb, and to improve BMI performance. In the first chapter of this work we try to shed some light on this debate. We show that ECoG channels contain substantial information about arm movement direction hence ECoG channels are directionally tuned. However, non-direct measures indicate that motor-unit activity might actually be better represented in the ECoG signal

2. Context specificity: Reaching for objects is one of the common activities we perform during our daily routine. Sometimes we reach for an object because we are instructed to do so (e.g. '…could you pass the salt please?') and sometimes we generate the movement internally without any external cue. By exploring the difference in neuronal activity when these two kinds of actions are performed we aim to advance our understanding of the mechanisms by which the brain controls the upper limb movements. Our overarching goal was to determine the extent to which brain signals recorded from the electrocorticogram (ECoG) can be used for a brain machine interface (BMI). Substantial evidence from scalp EEG and fMRI studies suggests that brain activity during cued vs. self-initiated movement is different. Several studies have attempted to dissociate neuronal activity of self-initiated and externally triggered voluntary movement (Tanji et al., 1988; Papa et al., 1991; Jahanshahi et al., 1995; Deecke and Lang, 1996; Hoshi et al., 1998; Pedersen et al., 1998; Yazawa et al., 2000; Cunnington et al., 2002; Hoshi and Tanji, 2004), and those studies found that there is a significant difference in the activity of cortical and sub-cortical areas during cued and non cued movement, as well as in the network configuration involved in these two tasks. Moreover, many studies argue that the

medial prefrontal cortex (MPFC) is more engaged during self initiated movement while the lateral prefrontal cortex (LPFC) has an important role in generating cued movement. Since the ECoG grid is usually placed on the LPFC and not on the MPFC it may well be that a BMI system acquiring signals from the LPFC will not be able to predict self initiated arm movements. Given that future BMI systems should operate in both conditions (self initiated and cued) we decided to test whether there is a difference in prediction accuracy while these two kinds of movements are preformed. In the second chapter I aim to address two basic questions on the difference between the cued and self-initiated movement using ECoG. First, I want to investigate whether ECoG recordings can be used to predict internally-generated arm movements as well as guided movement. Second I want to test if a system that was trained on one kind of movement will suffer from degradation in performance when applied to another kind.

3. Ipsilateral control: Current BMI systems are based on using functioning cortex capable of controlling the contralateral side of the body (Taylor et al., 2002; Wolpaw and McFarland, 2004; Leuthardt et al., 2006; Buch et al., 2008) and therefore offer little hope for patients suffering from hemispheric stroke. To enable hemiparetic patient the use of a BMI system it is necessary to facilitate a control using the unaffected motor cortex ipsilateral to the affected limb. The actual manner in which the motor cortex is involved with ipsilateral movements in humans is still not well understood. Nevertheless the idea that the motor cortex plays a role in ipsilateral movements has become evident in recent years. Functional MRI (fMRI) and positron emission tomography (PET) studies showed various levels of ipsilateral motor and motor-associated cortex are active with ipsilateral hand movements (Rao et al., 1993; Li et al., 1996; Catalan et al., 1998; Baraldi et al., 1999). Clinical studies have demonstrated that injury to motor cortex affects both contralateral and ipsilateral movements (Jones et al., 1989), indicating the involvement of ipsilateral cortex in motor control. To achieve a functional BMI for the future, an expanded understanding of how motor cortex participates in processing ipsilateral arm and hand movements is essential. In the third chapter of this work we provide evidence that signals recorded from motor areas of humans (ECoG) and monkeys (single-unit) can be used to reconstruct ipsilateral limb kinematics with high precision. Moreover, this representation can be used in a closed-loop BMI. These findings suggest the possibility of eventually creating fully functional BMIs for patients suffering from extensive unilateral hemisphere brain injury.

2 Complex directional tuning properties as revealed by human subdural recordings

2.1 Background

The seminal paper by Georgopoulos (Georgopoulos et al., 1982) initiated the study of directional tuned neurons in the primary motor cortex of monkeys. This approach has been used as one of the main tools to study movement-related cortical activity (Donoghue et al., 1998; Amirikian and Georgopoulos, 2003; Amador and Fried, 2004). Neuronal directional-tuning is defined as the change in average firing rate of a neuron when a subject's limb moves to a specific direction. Based on the notion that a population of directionally-tuned neurons can also predict a subject's movement direction intention, directional-tuning curves have become a corner stone of most modern BMI studies (Carmena et al., 2003; Hochberg et al., 2006; Ganguly et al., 2009). The most accurate control to date has been demonstrated from multi-regional multi-electrode arrays implanted in the macaque monkey cortex (Carmena et al., 2003; Velliste et al., 2008). This method has enabled the monkey to perform basic reach and grasp movement through BMI without the use of the animal's own limb. A similar approach performed on a quadriplegic human patient enabled the patient to perform various tasks including opening simulated e-mails, operating devices, and performing rudimentary actions with a multi-jointed robotic arm(Hochberg et al., 2006).

These results, achieved with ensembles of spiking neurons, encouraged others to demonstrate that directional tuning information can also be derived from multi-unit activity (Stark et al., 2009), as well as from local field potentials (LFPs) (Mehring et al., 2003; Rickert et al., 2005). Heldman, et al. (Heldman et al., 2006) found that almost 20% of LFPs recorded in motor cortex of monkeys during a standard center-out reaching task showed movement direction tuning in the high gamma spectral frequency band of LFPs (60–200 Hz). Little is known about the properties of neurons and LFPs in the homologous area (M1) of humans during normal movement due to the invasive nature of the single-unit approach. To our knowledge, only a recent single study, performed in a BMI setting for clinical purposes, showed that human (M1) neurons are also often directionally tuned (Truccolo et al., 2008).

The invasiveness of penetrating microarrays raises the question of whether comparable accurate prediction of direction can be achieved with less invasive methods. Electrocorticography (EcoG) involves recording from subdural surface electrodes. This method provides an alternative to the penetrating single-unit approach. It can potentially provide useful data about movement related activity from extended areas of the cortex and therefore may also be well-suited for the practical application of BMI (Leuthardt et al., 2004; Leuthardt et al., 2006; Pistohl et al., 2008; Schalk et al., 2008; Ball et al., 2009; Ganguly et al., 2009), However only few studies

have examined the specific properties of directional-tuning that can be derived from ECoG signals (Sanchez et al., 2008; Ball et al., 2009; Waldert et al., 2009).

Here we investigate the properties of directional-tuning curves of ensembles of neurons recorded using multiple ECoG electrodes. We find a complex distribution of cortical tuning based on hand movement direction. Electrodes showing non-directional tuning are driven by power in the intermediate frequency range. Electrodes showing directional tuning are associated with power changes in the raw time series, the delta band, and the high gamma band. We also show that two different movement directions can be decoded from the same ECoG channels by means of different temporal activation pattern. Finally, the tuning curve derived from single ECoG channels is flexible and can change over short temporal intervals. Taken together these results provide evidence that a distributed neural network involving directional and non-directional regions of the cortex supports goal-directed movement in humans.

2.2 Methods

Subjects: Two subjects (age 25-35 years) with refractory epilepsy were recruited from a pool of patients undergoing intracranial monitoring for the localization of an epileptogenic focus. Each patient had undergone a craniotomy for chronic (1-2 weeks) implantation of a subdural electrode array and/or depth electrodes. Electrode placement was determined on clinical grounds and varied between subjects (Figure 2). One subject was left handed (S1) and one was right handed (S2). The grids were placed in the hemisphere contralateral to the dominant hand.

None of the subjects manifested major cognitive deficits and antiepileptic drug therapy had been terminated during the week-long period of ECoG recording. The study protocol, approved by the UC San Francisco and UC Berkeley Committees on Human Research, presented minimal risk to participating subjects and did not interfere with the clinical ECoG recordings. All participants provided informed consent.

2.2.1 Data Recordings

The electrode grids used to record ECoG signals for this study were 64-channel 8 × 8 platinum–iridium electrodes (Ad-Tech Medical Instrument Corporation, Racine, Wisconsin). Electrode diameter was 4 mm (2.3 mm exposed), with 10 mm center-to-center spacing. Signals from the ECoG grids were sent to both a clinical monitoring system and a custom-recording system used for the experimental procedures described below. A broadband (256 channels, ~50 kHz) preamplifier (PZ2-256 256-Channel PreAmp, Tucker-Davis Technologies (TDT), Inc) was used to amplify the ECoG signals with the electrode furthest from the motor cortex used as a reference for all other grid electrodes. The amplified data were sent to an ultra-high performance data acquisition processor over a fiber optic connection (RZ2 Z-Series

Base Station, Tucker-Davis Technologies (TDT), Inc) that digitized the signal at 3052 Hz with 16-bit resolution.

Subjects used a stylus to perform arm movements on a touch-screen connected to a laptop computer. The stylus was registered as a mouse and the x-y position was sampled with custom-made MATLAB software (sampling rate > 70Hz). A PC-based, bus-powered USB device (Measurement Computing's USB-1208FS) was used to convert the mouse position to an analog voltage (1-4 V) and these voltages were sent to the analog input of the data acquisition processor (RZ2 Z-Series Base Station, Tucker-Davis Technologies, Inc) to be digitally sampled and stored together with the ECoG signals. During task performance, additional event markers (e.g. beginning of a trial, appearance of a target, acquisition of a target, etc.) were recorded from the digital ports of the PC-based bus-powered USB analog to digital convertor (Measurement Computing's USB-1208FS).

2.2.2 Behavioral task

Subjects were seated in a hospital bed with a touch-screen (KEYTEC INC.) placed in front in the horizontal plane. The subjects were asked to use a stylus to perform arm movements on the touch screen, with movements were mainly limited to rotations about the shoulder and elbow joints. They were instructed to minimize rotation about the wrist. All movements were made with the hand contralateral to the hemisphere containing the grid. For the purpose of another experiment (not reported here), we connected 4 rubber bands between the four corners of the touch screen and the stylus on some blocks. This manipulation generated a centro-symmetric resistive force; the subjects performed the same movements while reaching against the resistive tension imposed by the rubber bands.

The subjects performed several blocks of center out reaching task to 8 (or 6) targets on the touch screen. Each block lasted about 5 minutes and was composed of 240 (or 180) trials. A trial began with the appearance of a rectangular target at the center of the reach field. The subject then moved the stylus to the central location. Once that position was achieved, and following a delay of 0.6 ± 0.2 sec, a peripheral target appeared on the touch screen. These targets were arranged on a circumference of a 15 cm radius non-visible circle around the center target. Although the target locations were not marked on the screen, they remained fixed during the task. After a brief delay (100 - 500 ms), the center target disappeared. This served as the imperative signal, indicating that the subject should move the stylus to the target location. Once the stylus moved into the target location, the target disappeared, the center rectangle reappeared, the subject moved back to the center location. Each subject made 30 reaches to each target (total of 240 reaches), with the target location selected at random on each trial. We did not give specific instructions regarding eye movements. Based on observation, subjects naturally made a saccade towards the target prior to each hand movement.

2.2.3 Analysis

ECoG data, kinematic (position and velocity) variables, and discrete event markers (e.g. go cue, target position etc.) were continuously monitored and recorded. The kinematic data were stored with the ECoG data in the Multi-channel Acquisition Processor system (Tucker-Davis Technologies, Inc) for off-line analysis using custom-made MATLAB (MathWorks Natick, Massachusetts) software.

2.2.4 Preprocessing

The first step in our analysis included filtering, re-referencing, and down-sampling of ECoG signals. Line noise (60 Hz. and its harmonics) was removed using a notch filter and then re-referenced by subtracting the common average reference (CAR) from each electrode. CAR was calculated by averaging the raw signal of all the electrodes, omitting those that, upon visual inspection, had poor signal quality due to electrode drift, poor electrode contact or high frequency noise. The data were then bandpass filtered between 1 and 250 Hz and down-sampled to 500 Hz (Matlab function 'resample').

2.2.5 Time frequency decomposition

To generate event related spectrograms (ERS) plots we used a method similar to the one described previously (Canolty et al., 2007; Voytek et al., 2009). In brief, data were band-pass filtered across 10 frequency bands (4-7Hz 6-10Hz 8-12Hz 10-21Hz 13-30Hz 19-40Hz 31-59Hz 45-95HZ 61-120Hz 80-150Hz), using a Gaussian-shaped filter with a standard deviation of one-tenth the center frequency (CF), (full width half maximum of 0.2355 of the CF). The signal's envelope (analytic amplitude) per frequency band of the original series was extracted by the Hilbert transform. Each analytic amplitude was cross-correlated with another time series (with the same length) containing ones to mark the times of the events and zeros at all other times. This procedure resulted in a new time series (again, same length) that contained all the event-related potentials (ERP) for all possible time lags between the events and the analytic amplitude of a specific band-passed ECoG signal. The central section of the resulting vector was used as the 'real' ERP' while the other vectors were considered 'surrogate ERPs''. The 'real' ERP' was z-scored using the mean and standard deviation (SD) of the 'surrogate ERPs'' to create a normalized, or z-scored, ERP (Note, that while the raw analytic amplitude values are well-fit by a Gamma distribution, the mean analytic amplitude across epochs is well-fit by a Gaussian, in accord with the Central Limit Theorem). Since the standard deviation of the ensemble of 'surrogate ERPs' is a measure of the intrinsic variability of the across-epoch mean, it can be used to directly determine the uncorrected two-tailed probability of the deviation seen in the 'real ERP' at time t. It can be easily determined if the variation is due to chance or is correlated with the stimulus. For computational efficiency this procedure was computed in the frequency domain rather than in the time domain by using the convolution theorem. The full algorithm and MATLAB codes can be found in the supplementary material.

2.2.6 Electrodes classification

We defined three classes of electrodes:

1. Movement related but not directionally tuned: This class included electrodes that showed significant increase or decrease (alpha=0.01, $p<0.001$) in power, but the power did not change in a reliable manner for different directions. i.e., electrodes for which the standard deviation of power (across all directions) was less than half of the averaged power (across all directions).

2. Movement related and directionally tuned: This class included electrodes that showed significant increase or decrease (alpha=0.01, $p<0.001$) in power and showed strong variability of power for different directions. i.e., electrodes for which the standard deviation of powers across different directions was larger than half of the power average.

3. Neutral: Electrodes that did not show a significant increase or decrease (alpha=0.01, $p<0.001$) in power. These are omitted from further analysis.

Once an electrode was classified, we determined the times and frequencies at which the power crossed significance threshold. We then interpolated the measured power in the 8 cardinal directions of movement to 36 values (MATLAB function: resample (data,36,8) where the first point was appended to the data to avoid edge effects and removed after the interpolation). We determined the preferred direction of a channel at a specific time and frequency by: finding the angle of the maximum and minimum power. The preferred direction was defined as the angle of the maximum z-scored power (power>5 sd). If the z-scored power value was negative (power<-5) we defined the preferred direction as the angle of the minimum z-scored power+180 degrees.

2.3 Results

The two subjects were asked to use a stylus to perform center-out arm movements on the touch screen, with movements mainly limited to the shoulder and elbow joints. Both subjects performed the center-out movements without difficulty. The movements generally reversed in or near the randomly selected target and, as expected, were relatively straight with a bell-shaped velocity curve. The average time to complete a movement from the center to a target and back was 0.6 sec. Characteristic traces for one subject and the movement's profiles are shown in Figure 1

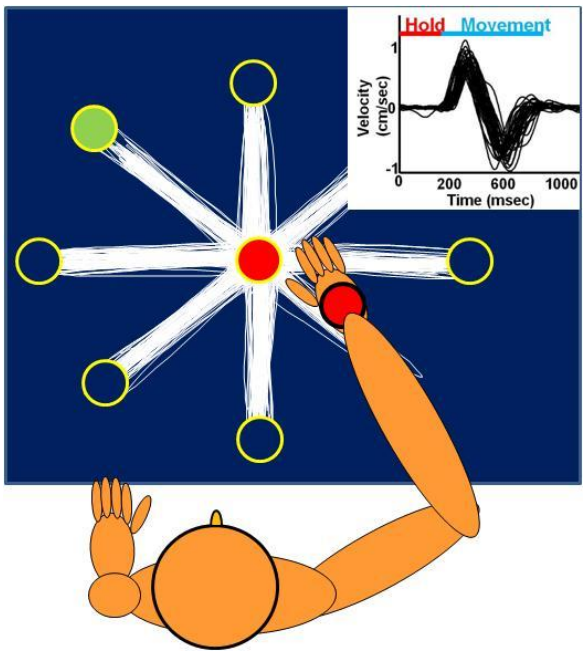

Figure 1 : Reconstructed trace of characteristic hand position and velocity profile of the task.

2.3.1 Movement Related spectrograms (non dir tuned)

To visualize movement related activity of ECoG signlas in various frequencies we generated Movement Related Spectrograms (MRS) and co-localized the results with the MR image of the subjects' brain (Figure 2, Figure 3).

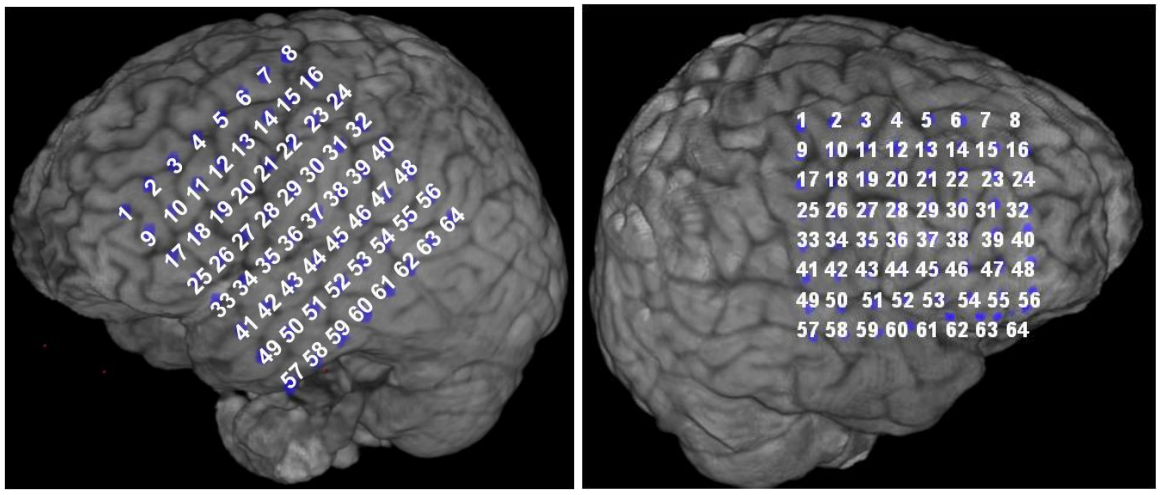

Figure 2 : ECoG electrode arrays with electrode numbers superimposed on 3D MR surface reconstruction images for subjects 1-2

The MRSs are calculated by passing the ECoG signal through several band-pass filters centered on a particular frequency. The output of each filter is Hilbert transformed (to extract the signal's envelope) and averaged across trials to obtain an estimate of

the instantaneous signal power at the filter's centre frequency. The band power estimates for all frequencies are combined to form a time–frequency map (see methods).

Movement related spectrograms (MRS) were first calculated by including all movements, independent of direction. We defined the movement onset as time zero and computed the MRS in a window of -500msec to +200mesc compared to 5000 surrogate runs. A representative MRS for all the electrodes can be seen in Figure 3 and in Supplementary figure 1; we only displayed MRSs of electrodes that crossed significance level (t-test alpha=0.001, p=0.0001 multi-comparison corrected). A stereotypical increase in amplitude power (often referred to as synchronization) can be seen in the high frequencies (f>50Hz) during the movement, preceded by a decrease in power (commonly referred to as desynchronization). The opposite phenomena (power decrease during movement is observed in the Beta freq (10<f<30). Task-related activation can be seen in electrodes located over sensorimotor cortex, dorsolateral prefrontal cortex, and parietal cortex confirming our MR X-ray co-localization.

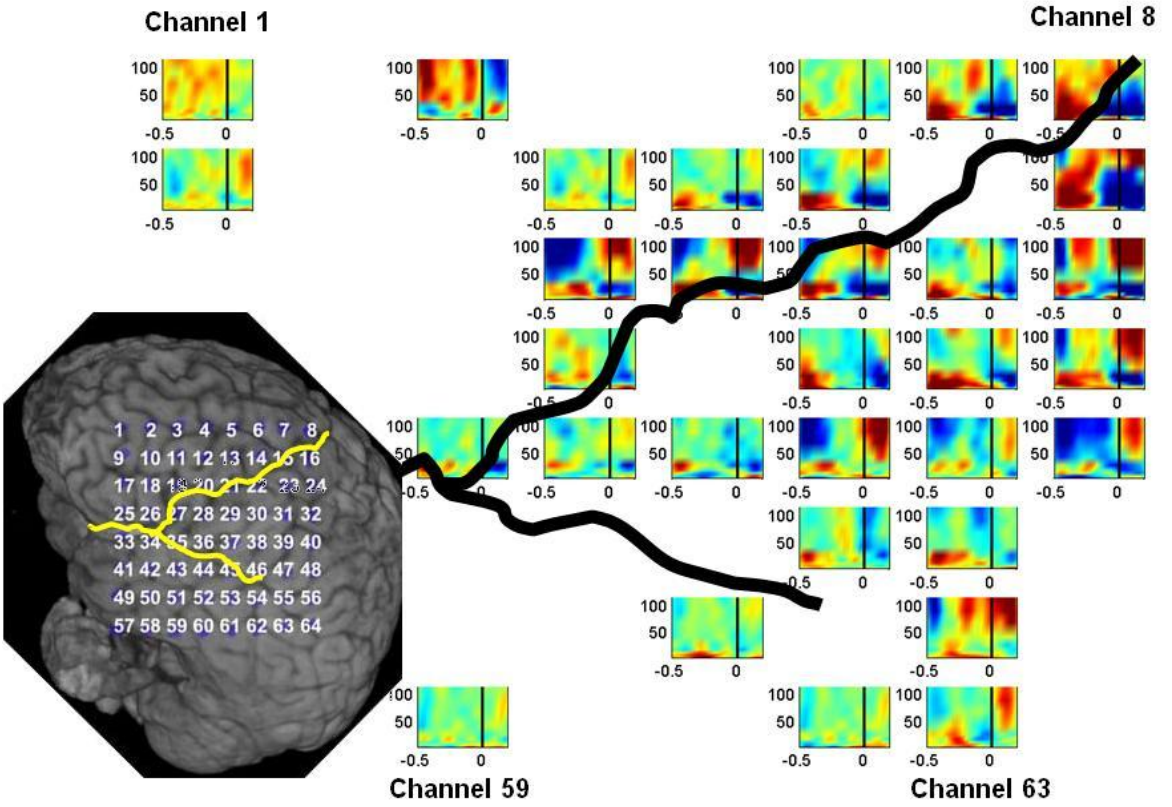

Figure 3 : Event-related time–frequency plots, time-locked to movement onset for Subject 1, the spectrograms are averaged over all movement directions. The location of the electrodes with the electrode number is depicted in the MR scan. X axis of each ERSP is time with 0 (vertical line) indicating movement onset. Y axis is frequency. Color code represent z-score values based on

permutation analysis (see methods). Electrodes with activations below significance threshold (t-test alpha=0.001, p=0.0001 multi-comparison corrected) are omitted.

2.3.2 Directional Tuning curves

To determine if cortical activity was related to movement direction, we determined the ECoG signal for each direction separately. Figure 4 and Figure 5 depicts significant changes in evoked potentials for each channel, with the octagonal shape indicating the directional tuning of the raw time series. Several frequency bands are overlaid over the MR scan. Electrodes that did not cross significance threshold in movement to any direction (t-test alpha=0.001, p=0.0001 multi-comparison corrected) were omitted from the figure. Each sector angle represents the averaged change in power (measured in SD compared to 5000 random permutations, see methods) over the course of hand movement to a specific direction. The radius of the octagon represents the time course of the hand movement with the inner and the outer most points corresponding to 500 msec prior and 200 msec after movement onset, respectively. We performed this analysis on the raw time series as well as on the analytic amplitudes (extracted using the Hilbert transform – see methods) of several frequency bands and the activation pattern for the 8 directions for each frequency band can be seen in Figure 4.

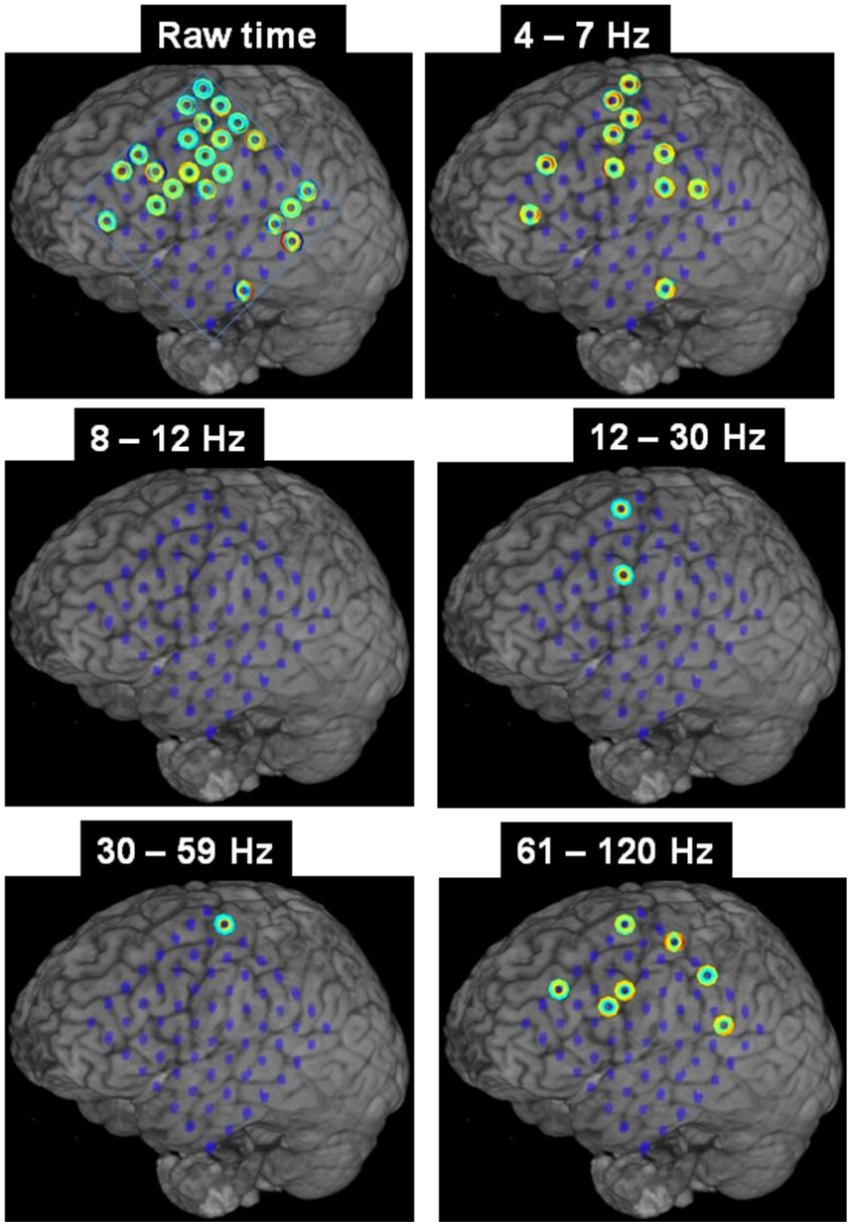

Figure 4: Directional tuning curves ECoG electrodes overlaid over the MR scans for Subject 1. Curves are shown for the raw-time series and five different frequency bands (4-7, 8-12, 12-30, 30-59, 61-120 Hz). Electrodes are omitted if significance threshold (t-test alpha=0.001, p=0.0001 multi-comparison corrected) was not crossed.

Some electrodes showed different patterns of activation as the hand moved in different directions, at least within certain frequency bands. These are referred to as directionally-tuned. Other electrodes showed a similar pattern of activation regardless of hand movement direction. These were classified as movement-related, but directionally non-specific.

Figure 5 shows a directionally tuned and a non-directionally tuned channel analyzed using the raw time-series as an input.

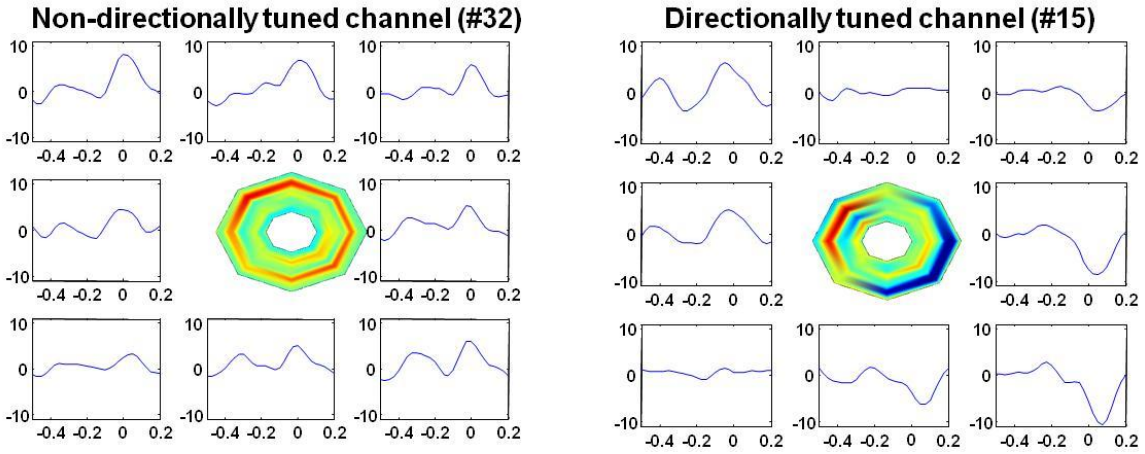

Figure 5 : Directional tuning curves (raw time series) for Subject 1, electrodes 32 (A) and 15 (B). The central octagon depicts the averaged change in power in 8 different directions. Surrounding graphs show cross sections of the curve in the 8 directions. X axis of each Surrounding graphs is time (0.5sec till 0.2 after prior to movement onset), Y axis is z-score values based on permutation analysis (see methods).

In panel A (channel 32) the activation level in all directions is similar throughout the time course of the hand movement. In panel B (channel 15) we see directional tuning; for example, there is a significant difference between movements to the upper-left and lower-right.

2.3.3 Spectral specificity of directional tuning curves

A dissimilar pattern of activation was found when we compared tuning curves between the raw time series and the analytic amplitude of several frequency bands. First, many electrodes that show a significant movement power change in the raw time-series did not exhibit significant activity when analyzed in the frequency domain. Second, the directional tuning was reduced (both in the number of channels and in the tuning depth) in the frequency domain compared to the raw time series analysis, similar to what was reported by Rickert et al. (Rickert et al., 2005).

Interestingly, ECoG signals may be tuned to one direction in one frequency band (or in the raw time series analysis) and to another direction in a different frequency band. Similar patterns of shift in directional tuning can be found in the time domain, i.e. an ECoG channel can be tuned to one direction 400msec prior to peak velocity and may shift its preferred direction at 200 mesc prior to peak velocity. An example of a channel exhibiting different preferred-directions in different frequency bands and different times can be seen in Figure 6

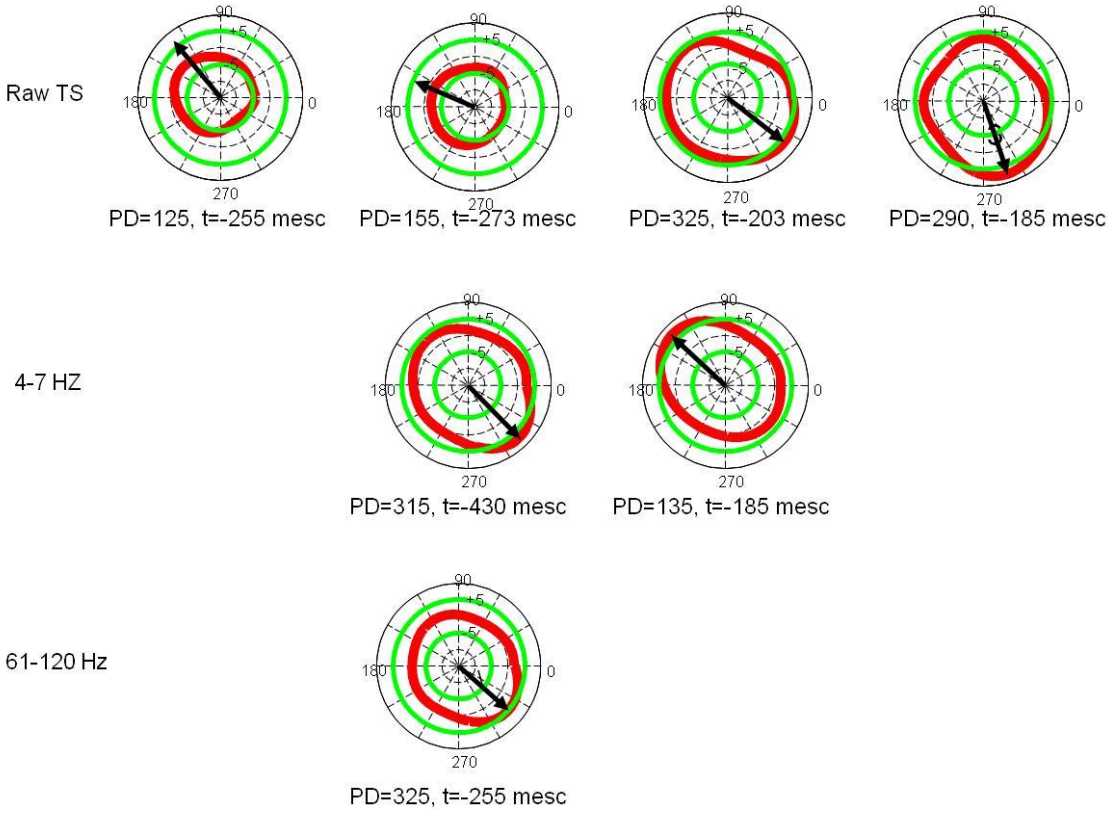

Figure 6 : Directionally tuned channel for Subject 1 Channel 3 exhibiting different directional preference in different frequency bands and times. The green circles in each plot indicate significance threshold, the red trace is the polar tuning curve (i.e. activation in Z-score units vs. movement direction) for a specific time and frequency, the black arrow point toward the max of the polar tuning curve or away from the minimum (in case that the minimum crossed negative significance level).

2.3.4 Preferred directions distributions in different spectral frequency bands for a single electrode

Figure 7 show the number of tuned vs. non-tuned electrodes in each frequency band. It can be seen that the raw time series and the delta band exhibit the largest number of directional tuned channels. Finally, we computed the distribution of preferred directions in different frequency bands over all channels. Note that a channel may be tuned to more than one direction in different times. If two or more preferred directions of a particular channel where 10 degrees apart or less (i.e. in different times) we considered them as one preferred direction. Figure 7 also show the number of electrodes that are tuned to each direction in any time point. It can be seen that the distribution of preferred-directions is not even and there are directions that are represented more than others but only one sector (240-270 deg) did not have any electrode tuned towards it.

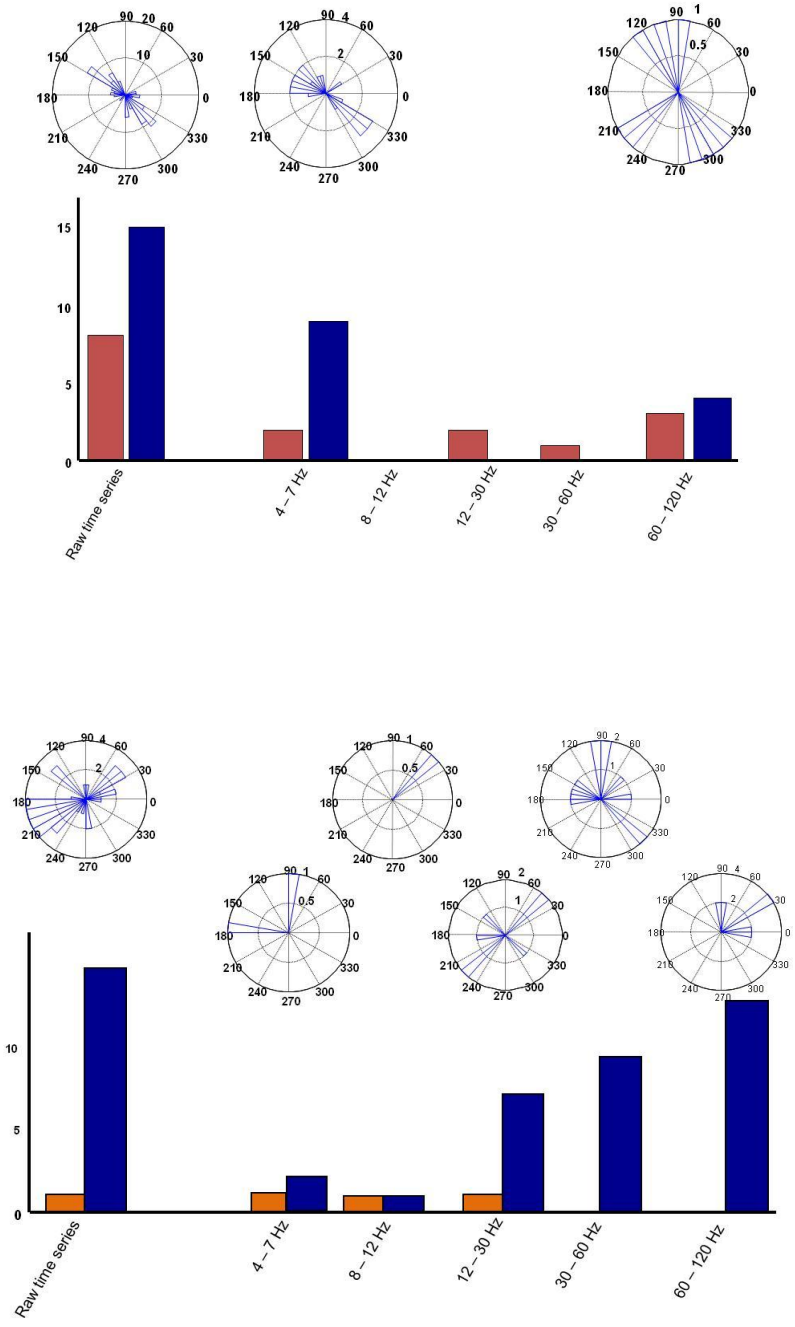

Figure 7 : Number of tuned and non-tuned electrode (subject 1 top subject 2 bottom). Blue bars show the number of tuned electrodes red bars show the number of non-tuned electrodes in each frequency band, maximum number of channels is 64. Polar histograms (above the bars) show the distribution of preferred directions in different frequency bands over all electrodes

2.4 Discussion

Movement evoked potentials (MEP) and movement related power changes in oscillatory activity of LFP and ECoG have been shown in several studies in monkeys (Murthy and Fetz, 1992; Sanes and Donoghue, 1993; Donoghue et al., 1998) and humans (Miller et al.; Crone et al., 1998a; Pfurtscheller et al., 2003; Leuthardt et al., 2004; Miller et al., 2007). Studies conducted in monkeys attempted to relate oscillations between 15 and 50 Hz to exploratory behavior (Murthy and Fetz, 1992), movement preparation, movement execution (Donoghue et al., 1998) and maintenance of a precise grip (Baker et al., 1999). Studies conducted in humans reported that high-frequency (30–90 Hz) power often increased during movements, whereas the amplitude of oscillations between 15 and 30 Hz decreased (Pfurtscheller et al., 1993; Aoki et al., 1999). Leuthardt et al. (Leuthardt et al., 2004) observed a direction-dependent increase in amplitudes in the high-frequency (40–180 Hz) band of human ECoG recordings during joystick movements in four different directions. Data from a hemicraniectomy model reported increased high gamma and decreased beta power during movement in accord with these findings (Voytek et al., 2009).

In our study we show that EGoG channels retain directional tuning information, similar to what has been found in studies involving single unit recordings or LFP measures (Donoghue et al., 1998; Mehring et al., 2003; Ball et al., 2009).

By examining ECoG tuning properties in the time domain, we show that ECoG tuning is manifested differentially in the power of different frequency bands. We also show that one channel may exhibit different preferred-directions in different times and that an ECoG channel have different direction tunings in different frequency bands. The finding that ECoG channels may contain directional tuning information may seem puzzling, given there are on the order of a million neurons contributing to the signal recorded in one ECoG electrode. Nevertheless one might predict that the activity of different neurons with different tuning curves will average out and no directional preference should be seen at the ECoG level. To explain these results we considered the following 4 hypotheses.

The partial distribution of neuronal preferred directions might not be random: If neurons sharing the same PD are clustered together, an ECoG chancel located over a cluster of preferentially tuned neurons should exhibit directional tuning properties. Such clustering has been reported in neurons in area M1 (Amirikian and Georgopoulos, 2003; Ben-Shaul et al., 2004; Stark et al., 2009) area V1 (Kamitani (Kamitani and Tong, 2005) and MT Tong (Kamitani and Tong, 2006) of monkeys as well as in fMRI voxels in the human cortex. If this hypothesis is correct it would not be surprising to find directionally tuned ECoG channels. However, we found that a large portion of the ECoG channels exhibit a very similar PD in the raw time series data and the power in the low frequency band in opposition to this hypothesis.

Conversely, the high frequency data supports this hypothesis. First, we found much broader distribution of different PD across channels in the high frequency data and second there are evidences that directly link the power in the gamma and high gamma bands to the firing rate of underling neuronal tissue (Feige et al., 2000; Nir et al., 2007). Thus, our data suggest that if such clustering of neurons sharing preferred directions exists it is mainly manifested in the activity of the high frequency bands.

Hypotheis two is that there are random fluctuations in the neural populations that are picked up by the ECoG channel. In this scenario, even though there is no clustering of preferred directions, an ECoG channel may be located over a local cluster due to chance fluctuations in power. In such a case all the preferred directions will be averaged out and the only remaining signal will be due to this random increase in one preferred direction population over all the others (Waldert et al., 2009). While we cannot rule out this possibility, it seems unlikely. First we find many channels tuned to similar directions and it is unlikely that this rare event (of non-equal distribution of directionally tuned neurons) will occur in several locations to a similar direction. Second, given the large number of neurons under each electrode and given the robust significance level of our directional tuned channels it is unlikely that a random fluctuation in the population would result in such a strong effect.

A third explanation is that the ECoG channels are correlated with muscle activity and not movement direction. It may be that the directional tuning of ECoG channels is an epi-phenomenon of encoding motor-units activity. If we assume that a power change of an ECoG channel is related to the number of motor-units involved in the movement, then hand movement to a direction that involves more motor-units will be categorized as preferred direction of such channel. For example, when using the left arm in 2D planar movements, movements to the front-left or rear-right (extension and contraction) involves mainly 4 major muscle groups (Biceps, Triceps, Pectoralis major, Deltoid), while movement to the front-right or rear-left (rotation about the elbow) involves mainly 2 major muscle groups (Biceps, Triceps). Many channels in our ECoG recordings showed this pattern.

Another piece of evidence arises from comparing the results of our two subjects. While in subject 1 the PD of a majority of the channels is to the front-left rear-right axis, the PD of a majority of channels in subject 2 is in the front-right rear-left axis see Figure 7. This is in accordance with the fact that the two subjects were using different arms to perform the movement (subject 1 – right arm, subject 2 – left arm). Note that this non-uniform distribution of PDs observed mainly in the MEP and in the delta band (1-4 Hz) and is not present in the activity of the higher bands. This may suggest that those two spectral domains represent different aspects of movement related activity.

Additional support for the motor-units hypothesis comes from the MEP data obtained (or the power increase in a certain frequency band) when the subject moved his arm against a resistive force (see methods). We found that the median MEP (and the

power in a certain frequency band) when the subject moved against a resistive force was greater than the median MEP when the subject did not move against a resistive force (Wilcoxon rank-sum test, alpha=0.001, $p<0.00001$). This increase was observed both in the directionally tuned neurons as well as in the non-directionally tuned ones. These results are also support the idea that the activity of neurons in the motor cortex represents muscle activity or muscle synergies rather than hand movement direction (Todorov, 2000; d'Avella et al., 2003; Pohlmeyer et al., 2007; Morrow et al., 2009).

Hypothesis four is that the tuning curves do not represent arm movement but rather a high level signal such as target location or directional attention. Our experiment was not designed to distinguish between tuning to direction of movement and tuning to target location. Previous studies have shown that directional tuning of motor and premotor neurons can occur without movement (Kalaska and Hyde, 1985; Georgopoulos et al., 1989; Wallis et al., 2001). The change in the tuning depth due to movement against a resistive force and the uneven distribution of the PD are not consistent with this hypothesis.

2.4.1 Relation between the high-frequencies, low frequencies and movement:

In our recordings, we found a different pattern of activity in the low, intermediate, and high frequency bands: the amplitude of the 16–42 Hz band decreased during movement execution, confirming previous results for monkeys and humans (Pfurtscheller et al., 1993; Sanes and Donoghue, 1993; Donoghue et al., 1998). Furthermore, in our study, the majority of the electrodes that showed movement-related activity in the raw time series and the low frequency band were also tuned to the direction of movement. In contrast, in the intermediate frequency band, very few of the electrodes showed directional tuning. We found a significant increase in high-gamma band activity around movement onset confirming other ECoG studies on humans (Crone et al., 1998a; Crone et al., 1998b; Pfurtscheller et al., 2003). Moreover, in our recordings, we also found that the power of some channels in the frequency band from 61–120 Hz was additionally modulated by the direction of movement and the preferred direction may be different than the one found in the PD of the raw time series and the low frequency band. When examining the distribution of PDs between the two bands (high and low) one can see that the strong directional preference of many electrodes observed in the low frequency analysis is absent in the high frequency data. We conclude that oscillations in the low frequency range, the intermediate frequency range and the high-frequency may reflect different functional roles in motor control. This difference in functionality of the two bands (high and low) was also observed in a recent study by Miller et al. (Miller et al. 2010)

Even though the activity in the intermediate frequency band was modulated by movement we did not observe strong directional tuning in this band. This is in agreement with the idea that this band related to more global and less specific involvement in the task such as attention modulation or target location. Some studies

suggest that high-frequency oscillations are a signature of combining movement primitives (considered as being represented by neuronal assemblies) into a complex movement (Murthy and Fetz, 1992; Donoghue et al., 1998). Additional studies are required to further differentiate between any of these possibilities for each respective frequency range.

In summary, while it is known that the cortex plays a critical role in the production of complex movements, it is debatable how motor commands and which motor commands are represented in different parts of the motor cortex (Mussa-Ivaldi, 1988; Scott, 2000b, c, a; Todorov, 2000) . Answering this debate is important to understand how the brain generates the large movement repertoire performed by the primate upper limb, and to improve BMI performance. Commonly, BMI systems extract kinematic parameters (position, velocity) from the neuronal activity and use this information to control the BMI, thus treating the primate's brain as a pure motion source. This makes intuitive sense considering that numerous studies show that neuronal activity in M1 and PMd can be correlated with higher-level features of hand movement such as position (Georgopoulos et al., 1982) and velocity (Schwartz, 1994; Moran and Schwartz, 1999).

It is also evident that the motor system directly modulates muscle activity (Evarts, 1968; Kalaska et al., 1989; Padoa-Schioppa et al., 2004) and numerous studies have shown that this modulation is essential for versatile interaction with the environment. We have shown that ECoG channels contain substantial information about arm movement's direction and that complex tuning properties can be found both in the time and frequency domain analysis. Thus, ECoG can be a good model to study neuronal correlates of movement and may shed light on the organization of the motor cortex in humans. This study bridges some of the gaps between the non-human primate laboratory and the human intracranial setting and suggests that neuronal ensembles recordings from human cortical motor regions may be able to provide informative control signals for BMI application. Moreover the clinical implications of this study are obvious in the rapidly growing field of brain machine interface.

3 Representation of arm kinematics in human cortex is context specific

3.1 Background

At the turn of the 21st century, Brain Machine Interface (BMI) research has made its way from the realm of science fiction to that of reality. Using signals obtained from movement-related cortical areas, non-human primates (NHP) and humans are able to control computers, wheel-chairs and robotic arms in real time (Serruya et al., 2002; Wolpaw et al., 2002; Carmena et al., 2003; Nicolelis et al., 2003; Wolpaw and McFarland, 2004; Hochberg et al., 2006; Velliste et al., 2008). Yet state-of-the-art BMI systems remain limited to basic and stereotypic movements. To date, human BMI research has been largely influenced by NHP studies in which the behavioral task consists of controlling a 2-d device to reach to an externally-cued target. Decoding algorithms, such as the Wiener filter, Kalman filter, or artificial-neural-networks are then used to reconstruct direction and/or velocity of limb movement from neuronal activity (Carmena et al., 2003; Hochberg et al., 2006; Leuthardt et al., 2006; Pistohl et al., 2008; Schalk et al., 2008). These decoding algorithms require an initial training stage to adjust the model parameters to the specific task and subject. In these studies, the performance of the BMI reconstruction model is tested on a new data set from the same task that was used to train the algorithm.

Neural representations of effector-related variables are observed in many regions of parietal and frontal cortex (Georgopoulos et al., 1982; Kalaska and Hyde, 1985; Kakei et al., 1999, 2001; Crutcher et al., 2004). While there remains considerable debate concerning the nature of these representations, an important observation is that the signals frequently show contextual affects (Donoghue et al., 1998; Hoshi et al., 1998; Asaad et al., 2000; Ben-Shaul et al., 2004; Crutcher et al., 2004). While such contextual specificity might not be surprising in prefrontal cortex, context-dependency is also observed in secondary and primary motor cortices (Hoshi et al., 1998; Hoshi and Tanji, 2004). For example, Donoghue et al. (Donoghue et al., 1998) showed that oscillatory activity in the gamma band (20-80 Hz) varied when the monkey performed cued vs. untrained, exploratory movements. These differences were evident even when the monkey performed similar gestures in the two conditions.

We address the general problem of context-specificity in the present study. Patients implanted with ECoG grids were required to perform two tasks, one in which they made center-out movements to visual targets and a second in which the movement trajectories were self-selected. We first asked whether the ECoG data could be used to train decoders in each task independently. Given that the grids spanned primary sensorimotor cortex, we expected that decoding would be successful for both types of movements. However, since the grids were placed on the lateral surface, it may be that a decoding algorithm based on the externally-cued movements would prove

superior to one based on internally-generated movements. Assuming that we would obtain accurate decoding reconstruction for both types of movement, we then turned to the context-specificity question. Specifically, can a model trained on one class of movements generalize such that it can reconstruct movement produced in the other context?

3.2 Methods

Subjects: Five subjects (age range 18–35 years) with refractory epilepsy were recruited from a pool of patients undergoing intracranial monitoring for the localization of an epileptogenic focus. Each patient had undergone a craniotomy for chronic (1-2 weeks) implantation of a subdural electrode array and/or depth electrodes. Electrode placement was determined on clinical grounds and varied between subjects (Figure 8 A-E). Three of the subjects were left handed (S1, S3, S5) and two were right handed (S2, S4). The grids were placed in the hemisphere contralateral to the dominant hand, except for subject 3 who had bilateral strips.

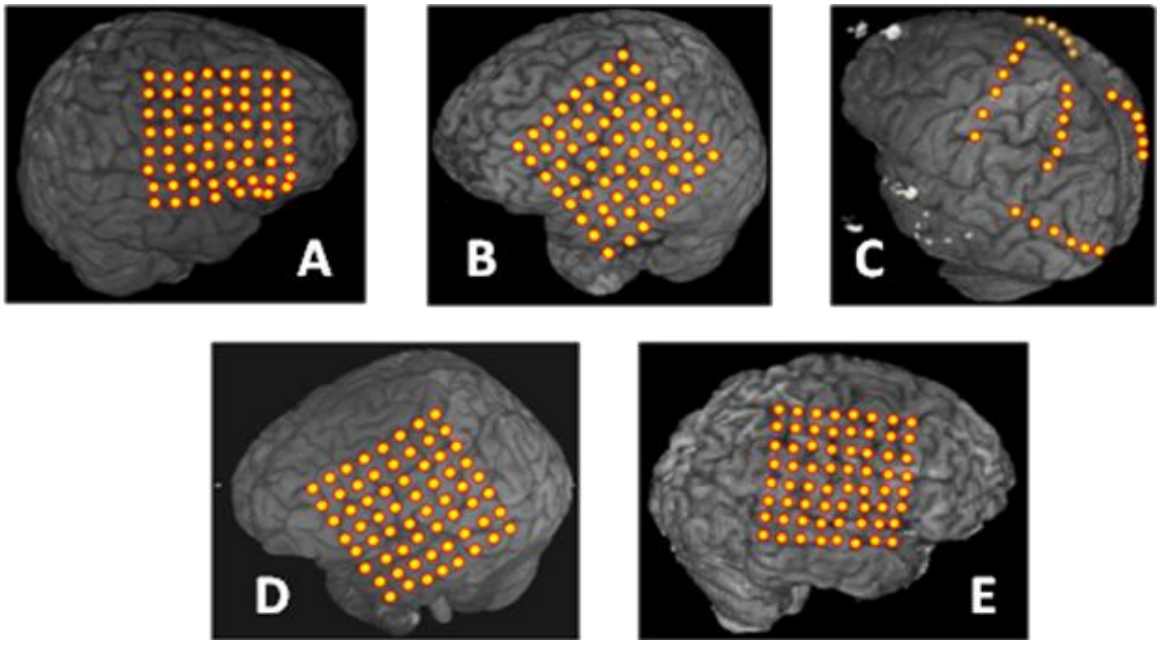

Figure 8: ECoG electrode arrays superimposed on 3D MR surface reconstruction images for subjects 1-5 (A-E)

None of the subjects manifested major cognitive deficits and antiepileptic drug therapy had been terminated during the week-long period of ECoG recording. The study protocol, approved by the UC San Francisco and UC Berkeley Committees on Human Research, presented minimal risk to participating subjects and did not interfere with the clinical ECoG recordings. All participants provided informed consent.

3.2.1 Data Recordings

The electrode grids used to record ECoG signals for this study were either 64-channel 8 × 8 (patient 1, 2, 4, 5) or 4 strips of 8x1 (patient 3) platinum–iridium electrodes (Ad-Tech Medical Instrument Corporation, Racine, Wisconsin. Electrode diameter was 4 mm (2.3 mm exposed), with 10 mm center-to-center spacing. Signals from the ECoG grids were sent to both a clinical monitoring system and a custom-recording system used for the experimental procedures described below. A broadband (256 channels, ~50 kHz) preamplifier (PZ2-256 256-Channel PreAmp, Tucker-Davis Technologies (TDT), Inc) was used to amplify the ECoG signals with the electrode furthest from the motor cortex used as a reference for all other grid electrodes. The amplified data were sent to an ultra-high performance data acquisition processor over a fiber optic connection (RZ2 Z-Series Base Station, Tucker-Davis Technologies (TDT), Inc) that digitized the signal at 3052 Hz with 16-bit resolution.

Subjects used a stylus to perform arm movements on a touch-screen connected to a laptop computer. The stylus was registered as a mouse and the x-y position was sampled with custom-made MATLAB software (sampling rate > 70Hz). A PC-based, bus-powered USB device (Measurement Computing's USB-1208FS) was used to convert the stylus position to two voltages (1-4V), one for X and the other for Y. These signals were sent to the analog input of the data acquisition processor (RZ2 Z-Series Base Station, Tucker-Davis Technologies, Inc) to be digitally sampled and stored together with the ECoG signals. During task performance, additional event markers (e.g. beginning of a trial, appearance of a target, acquisition of a target, etc.) were recorded from the digital ports of the PC-based bus-powered USB analog to digital convertor (Measurement Computing's USB-1208FS).

3.2.2 Behavioral task

Subjects were seated in a hospital bed with a touch-screen (KEYTEC INC.) placed in front in the horizontal plane. The subjects were asked to use a stylus to perform planar arm movements on the touch screen, with movements mainly limited to the shoulder and elbow joints. They were trained to minimize rotation about the wrist. The patients were instructed to keep the tip of the stylus in contact with the screen at all times. All movements were made with the hand contralateral to the hemisphere containing the grid (Subjects 1, 5 left, subject 3 both hands, subject 2, 4 right).

Each block was composed of two phases, one in which subjects performed externally-cued movements and one in which they performed internally-generated movements. The two phases were completed in one session and the subjects maintained their posture, as well as grip of the stylus, for the entire session (approximately 6 minutes). Subjects 1-5 performed blocks that included 285 sec (4.5 minutes for training and 45 sec for testing) phase of externally-cued movement followed by a 45 sec phase of internally-generated movement. Subjects 4 and 5 performed a second block in which they began with 285 seconds phase of internally-generated movement followed by a

45 sec phase of externally-cued movement. The description of the two tasks is detailed below.

EXTERNALY CUED- A center-out task was used for the externally-cued condition. Each trial began with the appearance of a rectangular target at the center of the reach field. The subject then moved the stylus to the central location. Once that position was achieved, and following a delay of 0.6 ± 0.2 sec a peripheral target appeared on the touch screen. These targets (6 or 8, depending on the participant) were arranged on a circumference of a 15 cm radius non-visible circle around the center target. The possible target locations were not marked on the screen but remained fixed during the task. After a brief delay (100 - 500 ms), the center target disappeared. This served as the imperative signal, indicating that the subject should move the stylus to the target location. Once the stylus moved into the target location, the target disappeared, the center rectangle reappeared, the subject moved back to the center location. Each subject made 30 reaches to each target (total of 180 reaches), with the position of the target selected at random on each trial. We did not give specific instructions regarding eye movements. Based on observation, subjects naturally made a saccade towards the target prior to each hand movement.

INTERNALLY GENERATED- In most blocks, the internally-generated condition was performed immediately following the end of the externally-cued condition. The transition was indicated when the display background turned yellow and a 15 cm radius circle appeared. The subjects were trained to freely move their arm about the touch screen while staying within the perimeter of the circle; the later was used to confirm that the movement's amplitudes were similar to the target directed condition. The subjects were explicitly instructed not to look at the screen. Beyond this criterion, we did not provide instructions as to where they should direct their eyes. The subjects generally kept their eyes open and either looked straight ahead or about the room while performing the internally-generated movements.

For the blocks that began with the internally-generated phase, participants were instructed to produce the free movements at the start of the block and to switch to the externally-cued condition when the background switched back to gray, along with the presentation of the center stimulus.

3.2.3 Analysis

ECoG data, Kinematic (position and velocity) variables, and discrete event markers (e.g. GO cue, target position etc.) were continuously monitored and recorded. The kinematic data were stored with the ECoG data in the Multi-channel Acquisition Processor system (Tucker-Davis Technologies, Inc) for off-line analysis using custom-made MATLAB (MathWorks Natick, Massachusetts) software.

3.2.4 Preprocessing

The first step in our analysis included filtering, re-referencing, and down-sampling of ECoG signals. Line noise (60 Hz. and its harmonics) was removed using a notch filter and then re-referenced by subtracting the common average reference (CAR) from each electrode. CAR was calculated by averaging the raw signal of all the electrodes, omitting those that, upon visual inspection, had poor signal quality due to electrode drift, poor electrode contact or high frequency noise. The data were then bandpass filtered between 1 and 250 Hz and down-sampled to 500 Hz (Matlab function 'resample').

3.2.5 Wiener Filter

We used a weighted linear combination of ECoG activity to reconstruct hand position and velocity. The basic form of this multidimensional linear regression algorithm or Wiener filter is:

$$m = \sum_i w_i N_i + b + \varepsilon$$

where $\boldsymbol{m}$ is a vector of positions and velocities at time t; $\boldsymbol{N_i}$ is an input vector of ECoG time-series signal at times *t, t-1, t-2… t-i*; $\boldsymbol{w_i}$ is a vector of weights; $\boldsymbol{b}$ is a vector of the DC shift; and ε is the residual error. Note that while lags in this equation can be negative (in the past) or positive (in the future) with respect to time t, we only considered lags into the past.

This equation can be written in matrix form as

$$m = wN$$

Each row in each matrix is a unit of time and each column is a data vector. The matrix **N** contains lagged data and thus has a column for each lag multiplied by the number of channels; e.g., 64 channels and 15 lags would correspond to 960 columns. The DC shift is handled by pre-appending a column of ones to matrix **N**. Matrix **W** is then solved by

$$w = (N^T N)^{-1} N^T m$$

In order to reconstruct the X-Y position of a movement from the ECoG data, we used the ECoG activity as an input to the Wiener filter. ECoG signals were band-passed into 9 frequency bands (1-8Hz 9-15Hz 16-30Hz 31-50Hz 51-70Hz 71-90Hz 91-110Hz 111-131Hz 131-150Hz), followed by calculating the analytic amplitude of each frequency band using the Hilbert transform. The resulting nine time-series were appended to the original time series of the ECoG signal, which generated a total of 64x10=640 ECoG channels. The 640 elements of this new time series were down-sampled to 15 Hz, and 1 s of ECoG data (15 bins) preceding a given point in time was used to train the model and generate reconstructions. We first tested the contribution

of each individual new time-series to the reconstruction of the hand movements, selecting as inputs to the Wiener filter those that produced the best reconstruction.

The model was trained using 4 min of data from the initial condition (Externally-cued: Subjects 1-5; Internally-generated: Block 2 for Subjects 4-5) and the reconstructive power was always tested using 45 sec of movement outside of the training window. First we tested within-context reconstructions by using the trained weights on 45 sec of the remaining data from the initial condition (Externally-cued: Subjects 1-5; Internally-generated: Block 2 for Subjects 4-5). To test context-dependency, we kept the weights fixed and tested the model's reconstruction against the movements produced during the last 45 sec of the block in which the subject performed in the novel context. The reconstructive power of each decoder was determined by comparison of neural reconstructions of X and Y position and velocity with that of the actual, measured values.

Similarity coefficient: To assess the accuracy of our model we defined a similarity coefficient (r_{SC}) that captures the resemblance between the real and the reconstructed movement.

$$r_{SC} = \sum_t \left(\frac{Signal_t^1}{N} \right) \cdot \left(\frac{Signal_t^2}{N} \right)$$

where

$$N = \max\left(\left\| signal^1 \right\|, \left\| signal^2 \right\| \right)$$

$$\left\| X \right\| \equiv \sqrt{x_1^2 + x_2^2 + \ldots x_n^2}$$

Measures of the correlation coefficient (CC) and percentage of variance accounted have been used as indices to calculate reconstructive accuracy in a number of BMI-related studies (Carmena et al., 2003; Pistohl et al., 2008; Schalk et al., 2008). The correlation coefficient, the PVA, and the similarity coefficient used here vary between 0 and 1, with a value of 1 representing two identical traces and a value of 0 representing two very dissimilar traces.

We found the similarity coefficient to be a better metric of reconstruction accuracy because, unlike the other measures, it does not result in large values when the two signals show a similar pattern but differ in scale (CC) or when the predicted signal is much smaller than the original one. Given that r_{SC} is always smaller or equal to CC or the PVA, this new metric is conservative.

3.2.6 Statistical Analysis

Bootstrapping was used to test for statistical significance of our results. We compared similarity coefficient (r_{sc}) distributions between real runs and randomly time-shifted data. This analysis also avoids any bias that might be introduced by

using a specific starting point. We constructed similarity-coefficient distributions by circularly shifting (MATLAB function circshift) both ECoG and movement data with a random shift 300 times. We found the best Wiener filter weights using the first 4 minutes of the shifted data and then applied this model to the remaining portion of the data. We applied this procedure, using both types of movements as the training set. The obtained weights were then used to reconstruct 45 sec of data from the same context, as well as from the other movement context. This process resulted in a distribution of r_{SC} for each block and each movement parameter (X-pos, Y-pos, X-vel, Y-vel). A Wilcoxon signed rank test was used to compare the actual runs to 'chance' runs. To generate 'chance' runs we created a random lag between the movement and the ECoG data. Again, we circularly shifted the ECoG data 300 times with a random shift, except this time, we did not shift the movement data to obtain the best Wiener filter weights that were then used to test the remaining data set. The result of this procedure is another distribution of r_{SC} for each block that is referred to as a 'chance' distribution.

3.3 Results

The center-out movements used for the externally-cued phase of training were performed without difficulty. The movements generally reversed in or near the targets and, as expected, were relatively straight with a bell-shaped velocity curve. In the internally-generated phase, participants tended to produce curved, continuous movements. Characteristic traces from the externally-cued phase and internally-generated phase for one subject are shown in Figure 9 (A, F). Hand movements were faster and more evenly distributed over the working space during the internally-generated phase. Nevertheless, as can be seen in Figure 9 (B-E, G-J) the range of movement in both the x and y directions was similar for the two phases.

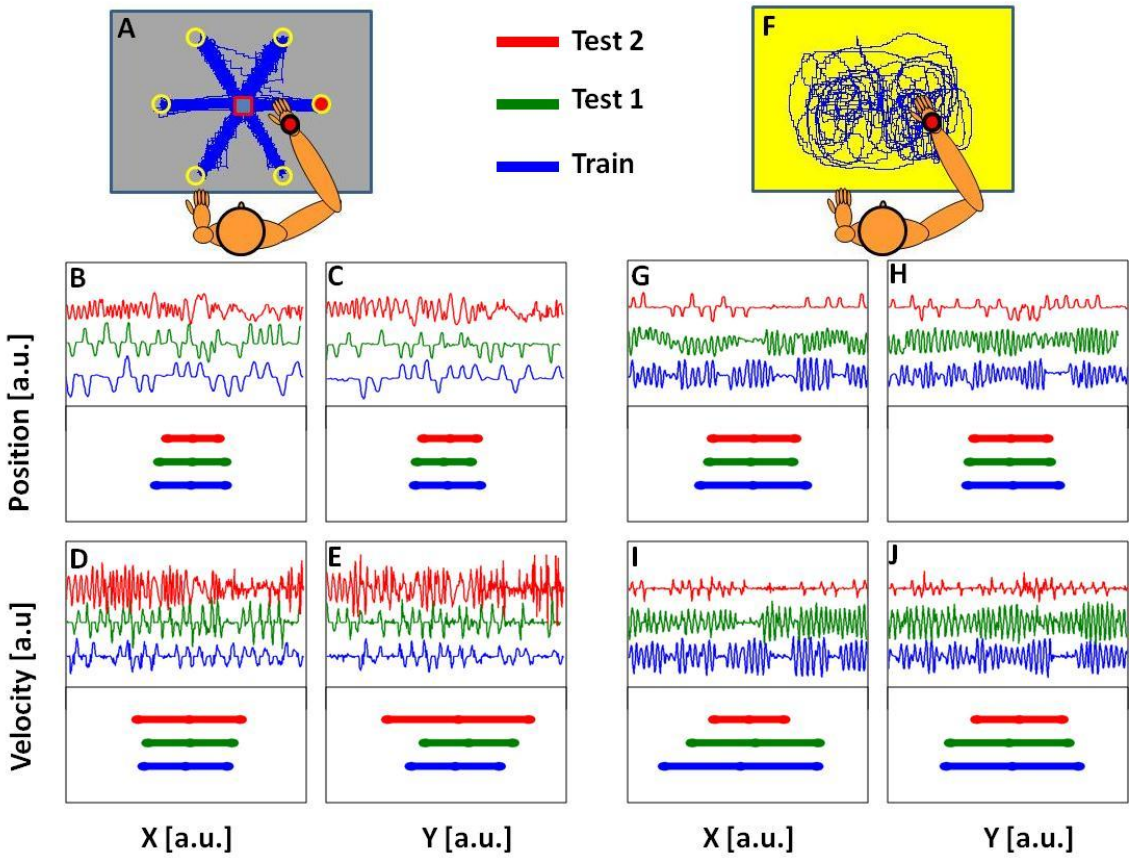

Figure 9: Reconstructed traces (A, F) and spans of hand position and velocity for the externally-cued condition (left side, A-E) and internally-generated condition (right side, F-J).

3.3.1 Decoding accuracy within context

Using an algorithm based on a Wiener filter, we were able to reconstruct arm movement with reasonable accuracy. We first tested whether a Wiener filter trained with data from one type of movement could reconstruct movement from a subsequent epoch of that same condition; that is, we tested the reconstructive ability

of the model on data from the same movement condition but had not been used to train the model. To this end, using the ECoG signals, we trained a Wiener filter model using 4.5 min of the data set. With the weights fixed, we then tested the model with 45 s of data that had been excluded from the training set. A representative reconstruction of hand trajectory is depicted in Figure 10 A, D. The black trace shows the actual X and Y coordinates of hand position as recorded by the TDT system. The red trace is the reconstructed hand position from the ECoG signals. The group averaged r_{SC} values for the externally-cued and internally-generated movements were 0.50 and 0.47, respectively. Similar results were obtained when we used hand velocity (rather than position) as an input to the Wiener filter (Supplementary figure 2 E, F)

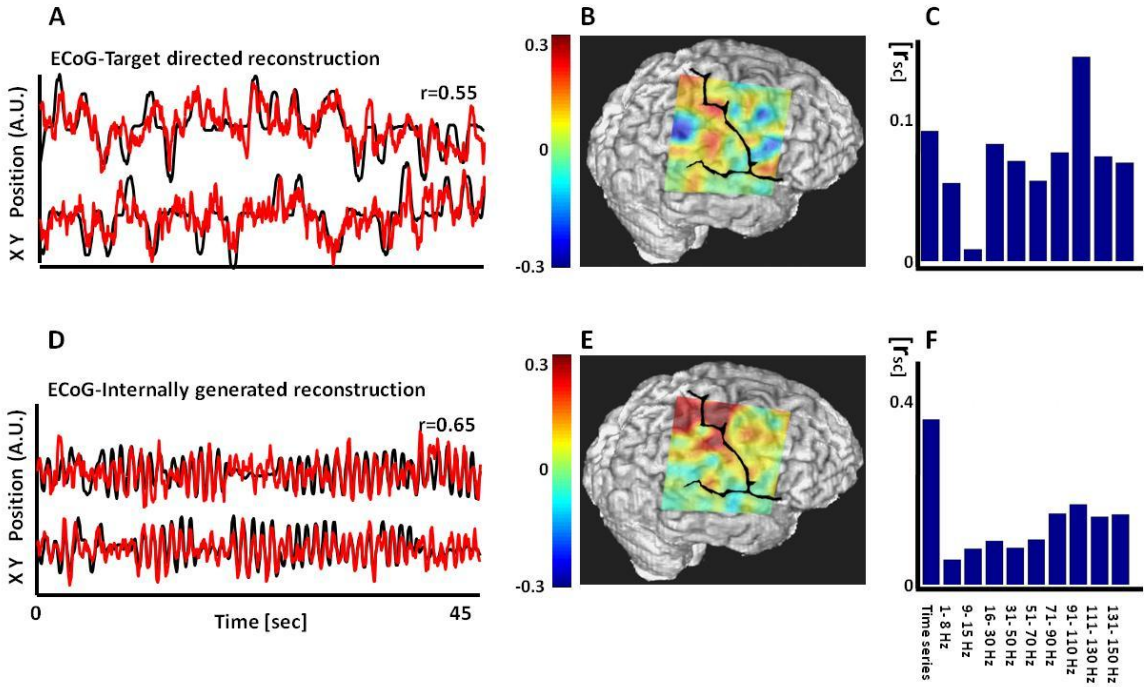

Figure 10: Comparison of observed hand position and reconstructed hand position based on a model derived from ECoG data. The reconstructions were always generated for 45 sec of data from the same movement condition that had been excluded from the training data set (A.U. means arbitrary units). Upper row: Externally-cued condition. Lower row: Internally-generated condition. Left column (A, D): Black traces show hand position across time and red traces show the ECoG-based reconstruction of hand position for a representative 45 s segment. The r value is the similarity coefficient between the reconstructed and the actual traces (averaged Activation maps

To evaluate the contribution of individual electrodes on decoding accuracy, we calculated individual electrode r_{sc} values for each grid. Representative maps displayed over MRI scans are shown in Figure 10 B, E. Electrodes located over M1 and dorsal premotor cortex contributed more to the reconstruction of movement than other sites (see Figure 10 B, E). We also assessed the contribution of individual frequency bands to reconstruction accuracy. No single band stood out in a qualitative

assessment (see Figure 10 C, F). Rather, in most cases, the raw time series provided the strongest contribution to accuracy, similar to that reported by Schalk et al.(Schalk et al., 2007) Across the frequency spectrum the highest contribution to reconstruction accuracy was generally observed in the high gamma band, consistent with other reports (Miller et al., 2007; Pistohl et al., 2008).

3.3.2 Generalization to a novel context

To evaluate context-specificity, we next asked if the ECoG decoding algorithm could generalize to the novel task context. For all subjects (5 subjects, total of 19 blocks), a Wiener filter model in which the weights were fixed from data obtained during 4.5 min of externally-cued movements was used to reconstruct 45 s of internally-generated movements. For two of these subjects, we also used the reverse test of generalization, fixing the weights from the first 4.5 min of internally-generated movements and using this model to reconstruct a subsequent 45 s phase of externally-cued movement.

As noted above, when the Wiener filter was trained on the externally-cued movement, the group average similarity-coefficient (r_{SC}) for reconstructed movements produced in the same context was 0.5 (sd 0.08). When the same model was used to reconstruct internally-generated movement from the same block, the group average r_{SC} fell to 0.13 (sd 0.09), a value that was reliably different from the reconstruction for the external phase of that block (Wilcoxon signed rank test n=19, α=0.05, p= 0.00013). The group average results are depicted in Figure 11 E, F (see also, Supplementary figure 2 E, F). Similar results were obtained when the data were analyzed on a subject-by-subject basis. The averaged r_{SC} for externally-cued movements were larger for each subject in comparison to averaged r_{SC} for internally-generated movement. The individual values for the five subjects on externally-cued epochs were 0.44, 0.53, 0.59, 0.36 0.47. The corresponding values on internally-generated epochs were 0.14, 0.15, 0.24, 0.06, 0.06.

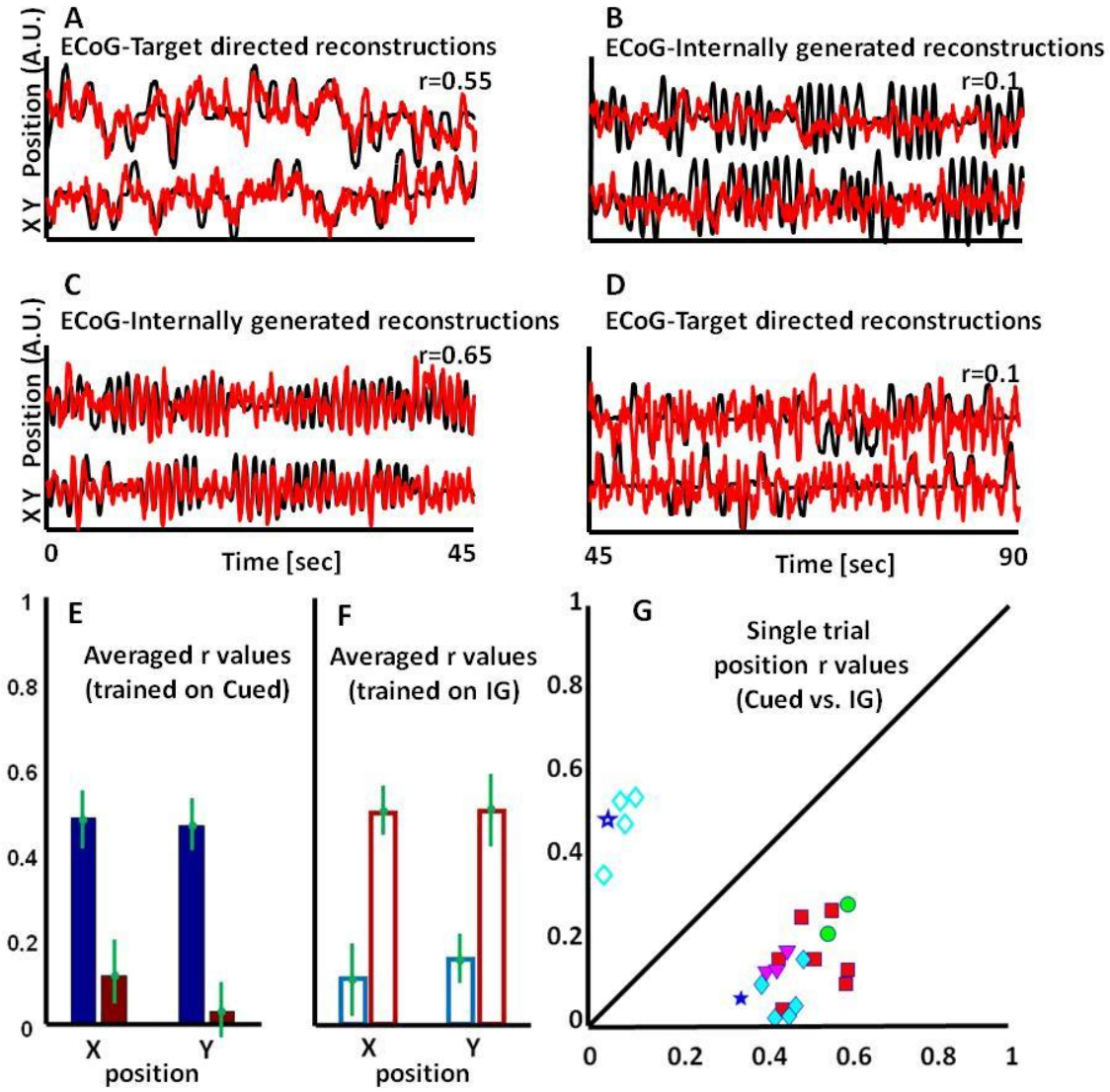

Figure 11: Generalization test of ECoG-based model. Comparison of observed and reconstructed hand position based on a model derived from ECoG data (A.U. means arbitrary units). Upper row: Model with externally-cued condition as training set used to reconstruct hand position for same condition (A) or internally-generated condition (B). Middle row: Model with internally-generated condition as training set used to reconstruct hand position for same condition (C) or externally-cued condition (D). The traces and r values are as described in Figure 10. (E-F) Grand average of similarity coefficients between the reconstructed and actual traces. Blue bars: reconstructed externally-cued movement; Red bars: reconstructed internally-generated movement. G) Similarity coefficients for the two movement conditions from individual blocks. Solid and empty marks are data points derived by training the model on externally-cued and internally-generated condition respectively. The X value is the r_{SC} for reconstructing externally-cued movement and the Y value is the r_{SC} for reconstructing internally-generated movement. Colors indicate different subjects.

We also tested whether the ECoG signals obtained during the externally-guided phase could reconstruct movement during the internally-generated phase on a block-by-block basis. Representative traces of the two conditions are shown in Figure 11 A, B

(see also Supplementary figure 2 A, B). A close match is apparent between the actual and reconstructed movement during the externally-cued phase. In contrast, a poor match is seen between the two traces during the internally-generated phase. A scatter-plot comparing the block-by-block similarity coefficients for the two conditions is shown in Figure 11 G (and in Supplementary figure 2 G). As seen from the plot, all of the solid data points fall below the unity line, the function for which reconstructive value would be identical for the two conditions. Thus, in every block, the r_{SC} values obtained for the externally-cued movement were larger than the r_{SC} values obtained for the internally-generated movement when the Wiener filter was trained with externally-cued data.

A similar pattern was observed in the more limited generalization test in which the model was trained with data from an extended internally-generated phase and then used to reconstruct an untrained segment of internally-generated movement or externally-cued movement (2 subjects, total of 5 blocks). The group average r_{SC} values for internally-generated and externally-cued movements were 0.47 (SD=0.1) and 0.07 (SD=0.05), respectively (Figure 11 F and Supplementary figure 2 F). Statistical analysis confirmed that the difference between the two conditions was reliable (Wilcoxon signed rank test n=5, α=0.05, p=0.04). These values were essentially the same when the data for the two subjects were analyzed separately. A representative trace from a block-by-block analysis is depicted in Figure 11 C, D and the similarity coefficients for the data pairs are included in the scatter plot of Figure 11 G (see also Supplementary figure 2 C, D and G). These pairs all lie above the diagonal; hence, in every block when the Wiener filter was trained on internally-generated movement, the r_{SC} obtained for the internally-generated movements were larger than the r_{SC} obtained for the externally-guided movement.

3.3.3 Control analysis of generalization assessment

As a further statistical analysis, we compared similarity coefficient distributions between real runs and randomly time-shifted data. This analysis avoids biases that might be introduced by using specific starting points. We found that the real-shifted distributions were different than the chance-shifted distributions (Wilcoxon signed rank test, n=300, α=0.05, p<0.00001,). However, when the Wiener filter was trained on one mode of movement and then tested on the different mode (trained on internally-generated and tested on externally-guided and vice versa) the distribution of r_{SC} was not different from chance (Figure 12).

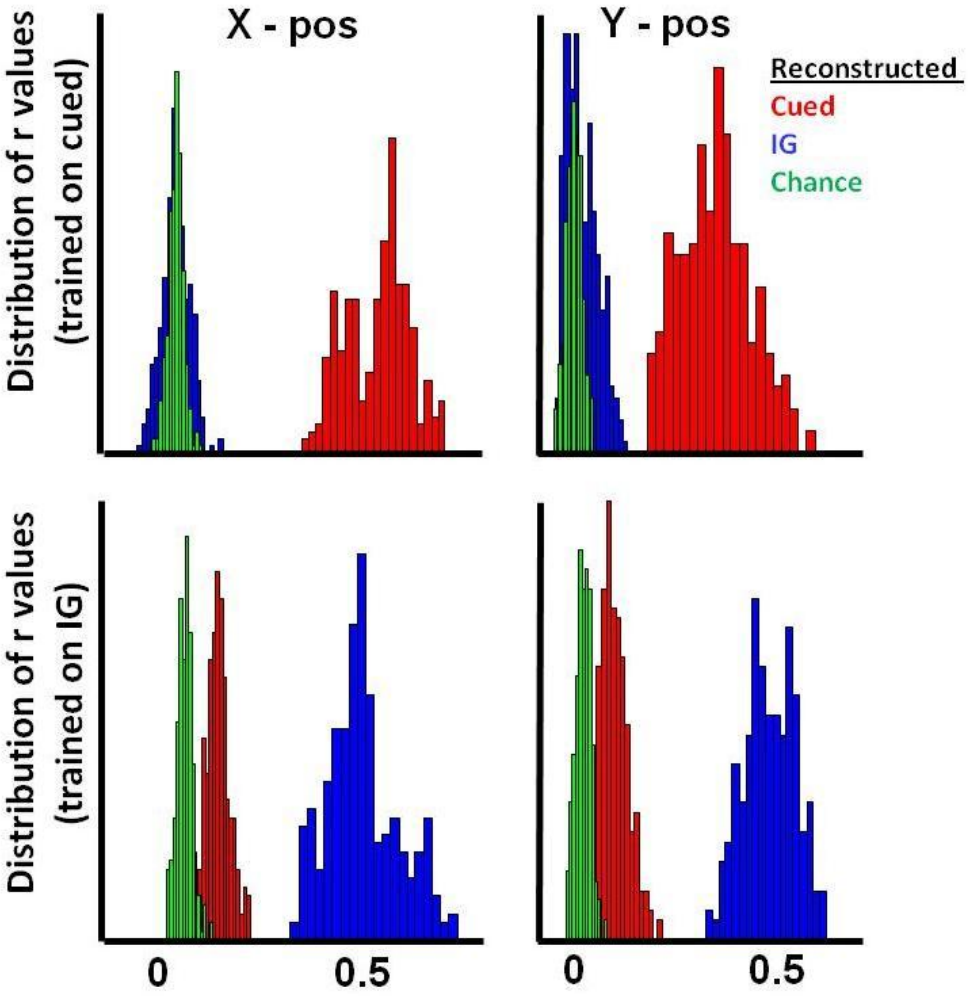

Figure 12: r_{sc} distributions for actual runs and chance runs used in the bootstrapping analysis. Top panels show data from a model trained on externally-cued movements and lower panels show data from a model trained on internally-generated movement. Red histograms are reconstructed r_{sc} for externally-cued movement, blue histograms are reconstructed r_{sc} for internally-generated movement, and green histograms are chance runs.

3.4 Discussion

This study demonstrates that ECoG neural signals can be used to reconstruct both internally-generated and externally-cued continuous hand movement. We were able to make reasonably good within-context reconstructions of 45 s of untrained data by devising a reconstruction algorithm (e.g. Wiener filter) based on 4.5 min of training data from the same condition. This procedure was successful for all five subjects even though there were considerable differences in the coverage of the ECoG grids. The accuracy of the reconstruction was not only similar between subjects, but also between different blocks within a single subject.

A novel feature of our study was the assessment of generalization between externally-cued and internally-generated modes of movement. To address this, we tested whether ECoG signals obtained in one mode could reconstruct continuous arm movement performed in the other mode. The results showed a marked reduction in reconstruction accuracy in the generalization tests. Indeed, using weights acquired in one mode resulted in similarity coefficients that did not exceed chance when applied to movements produced in the other mode. This observation indicates that Weiner-filter training weights are context-specific.

3.4.1 Specificity of movement training weights

The reduction in reconstruction accuracy across tasks may be related to the differential contribution of frontal and parietal regions to the control of externally-cued and internally-generated movement. Several EEG studies have attempted to dissociate neuronal activity of self-initiated and externally triggered voluntary movement (Papa et al., 1991; Jahanshahi et al., 1995; Deecke and Lang, 1996; Gerloff et al., 1998; Pedersen et al., 1998; Thut et al., 2000; Yazawa et al., 2000; Weilke et al., 2001; Cunnington et al., 2002). Thut et al.(Thut et al., 2000) found that, although movement selection evoked similar surface potentials independent of whether a movement was externally-cued or self-selected, these potentials differed in duration depending on the selection mode. Similarly, Gerloff, et al.(Gerloff et al., 1998) showed that functional coupling in the beta frequency range was enhanced during internally paced finger movements in comparison to cued finger movements. They suggested that internally paced movement poses higher demands on the motor system, leading to increased regional activation and an enhancement of information flow between the premotor and the sensorimotor areas of both hemispheres. Moreover, activations in subcortical structures including basal ganglia, cerebellum and thalamus, vary as a function of movement context, and this will influence their impact on cortical activity (van Donkelaar et al., 1999; Vaillancourt et al., 2003). As noted in the Introduction, LFP oscillations in a motor cortex of a monkey are strongly modulated by the context in which the task is performed (Donoghue et al., 1998). Given that the LFP oscillations were only loosely correlated with neuronal firing rates, the authors proposed that the fast LFP oscillations may represent processes that are not related to specific aspects of movement but rather to more abstract or global features of action goals. Taken together these studies are consistent with the notion that ECoG signals may markedly differ during similar gestures as a function of context.

The relationship between neuronal firing-rate and ECoG activity remains unclear (Nir et al., 2007; Ray et al., 2008). Some studies suggest that ECoG signals are better linked to synaptic activity rather than to the neuronal firing rate (Freeman and Skarda, 1985). Another hypothesis is that ECoG oscillations may help establish long-range synchrony among cortical neurons (Schoffelen et al., 2008). These hypotheses suggest that, while similar movement patterns might generate similar activity patterns in the single unit level (action potentials), ECoG patterns may be context specific even during similar gestures.

This electrophysiological evidence suggests that motor cortex activity is modulated by the task rules, task objectives, and task demands. The degree to which movement-related cortical activity is modulated by the task-context in humans remains unclear (Sochurkova et al., 2006). Goal-directed and self-initiated movements provide a starting point to explore contextual effects. Similar kinematics may be used to either reach to a target location or produce a gesture in the absence of an external cue, yet the different contexts may have a significant influence on the neural coding of the movement. Indeed, a large body of literature has described differences observed with PET, scalp EEG, and fMRI between externally-cued and self-initiated movement (Jahanshahi et al., 1995; Cunnington et al., 2002; Gowen and Miall, 2007; Habas and Cabanis, 2008). One theme emphasized in many of these studies is the hypothesis of a lateral-medial gradient of control: Medial prefrontal cortex (MPFC), including supplementary motor area (SMA), is more strongly engaged during self-initiated movements whereas lateral prefrontal (LPFC) and premotor cortex are more strongly engaged during externally-cued movements (Gerloff et al., 1998; Deiber et al., 1999; Yazawa et al., 2000; Crutcher et al., 2004; Kurtzer and Scott, 2007; Bestmann et al., 2008). However, this dichotomy has not been supported by other studies (Amador and Fried, 2004; Hoshi and Tanji, 2004). The hypothesized distinction between lateral and medial cortex is particularly relevant when evaluating the viability of ECoG for BMI control since ECoG grids are more commonly placed on the lateral surface of the cortex.

3.4.2 Potential biases

There are also important methodological differences between the externally-cued and internally-generated movement conditions and the failure of generalization may, at least in part, be related to this. First, planning is relatively constrained in time during externally-cued center-out movements. In contrast, planning is presumably ongoing and less constrained during the internally-generated task. Thus, ECoG activity during the latter may reflect the processes that are completed when there is time to prepare movement, but overlap movement when preparation, attentive-related processes, and movement must be simultaneously processed.

Second, we must consider whether the lack of generalization is related to differences in kinematics between the two tasks. Are the statistical distributions of hand position and velocity sufficiently similar? The Wiener filter, as well as many decoding algorithms, will not generalize well if they are trained in one part of the kinematic space and tested in another. Thus, a lack of generalization would not be surprising if there were significant kinematic differences between the two conditions.

While there are clearly kinematic differences, we do not believe these can account for the poor inter-task generalization. The X and Y data were treated separately with the Wiener filter algorithm, finding the best weights to reconstruct the movement in each axis independently. Although the spans of X, Y, Vx, Vy (Figure 9 A-J) are different between the two tasks, the ranges are similar except for the edges of the kinematic

workspace. If sampling space was important, we might expect the failure of generalization to be most pronounced for these extreme positions. This was not the case: models trained with externally-cued movements failed to reconstruct internally-generated movement across the workspace.

Hand velocity in the internally-generated task was sometimes higher than in the cued task. If generalization requires that the decoding algorithm span the range of test values, then we might expect to see an asymmetry in that the Wiener filter trained with data from the internally-generated task would be able to reconstruct externally-cued movement. However, there was no evidence of such an asymmetry. Generalization failed similarly in both tests.

Nonetheless, we conducted a simple simulation to explore the effects of kinematic differences. We simulated ECoG signals using movement information, and used this to reconstruct hand position and velocity. We used real X and Y kinematics (position, velocity) and added a large amount of random noise (signal to noise 1:50) as well as some random time lags. The resulting signal was used to generate 64 simulated ECoG channels; that is, these signals contain the movement kinematics, but this information is now embedded in lots of noise. We then used a subset of only the externally-cued segment as a training set and used the resulting data to predict real movement (both externally-cued and internally-generated), similar to what we have done with the real ECoG data. Importantly, the movement reconstruction using the simulated data was comparable between the two tasks (SC=0.57, externally-cued; SC=0.52 internally-generated); that is, we obtained good generalization. This simulation demonstrates that kinematic differences between the two tasks are not sufficient by themselves to account for the reduction of prediction accuracy in the inter-task tests based on real ECoG signals (Supplementary figure 3).

Another methodological difference relates to eye position and eye movements. During the externally-cued movements, subject typically moved their eyes to the target along with the arm movement. These targets were not present during the internally-generated phase and, in fact, the subjects were specifically instructed to not look at their hand. It is possible that the algorithm was actually decoding information about eye movement/position rather than arm movement/position.

We cannot rule out this hypothesis given that our ECoG recording setup did not include the measurement of eye movements. However, two features of the results are at odds with an eye-movement account of the lack of generalization. First, when the Wiener filter was trained with internally-generated movement, good reconstruction was observed on data from the untrained phase for this condition. Second, at the end of one session, we had one subject (S4) perform a tracking task. In this task (run after the main experimental block), a blue dot was visible on the screen. It followed the same trajectory that had been produced by the subject during the internally-generated phase of that block. The subject tracked the blue dot with the stylus. Wiener filters, trained with either the externally-cued or internally-generated phases,

were used to reconstruct performance during the tracking phase. Accuracy was poor for either filter. Thus, we failed to find generalization between tasks with similar eye movement control (externally-cued and tracking) as well as between tasks with similar kinematics (internally-generated and tracking). We note that eye movements have not been used in most previous studies examining movement decoding. Any limitation with our data would also apply to these studies.

3.4.3 Conclusion

Our study demonstrates that continuous hand position, based on either internally-generated or externally-cued movement can be decoded from ECoG signals. However, the results show a surprising lack of generalization between these two modes of control, suggesting that the decoding algorithms are highly context-specific. Even when movement trajectories are similar, contextual features of the movement influence neuronal activity, both within a cortical region and the interactions between cortical regions, at least when measured at the meso-scale of ECoG. This finding suggests that it is not hand movement or position per-se that is decoded from the ECoG signal, but rather a combination of information that incorporates more global parameters such as the task goal, form of control, and reward structure of the task.

BMI holds great clinical value for amputees and patients with spinal cord injury, stroke, and neuromuscular disorders. It will become increasingly important to further develop signal analysis techniques and derive effective transform algorithms for translating neuronal activity into reconstructive and meaningful motor parameters for BMIs. For such algorithms to be of therapeutic utility, it will be important to solve the problem of context specificity.

4 Cortical Representation of Ipsilateral Arm Movements in Monkey and Man

4.1 Background

While the main organizational principle of primate motor systems is cortical control of contralateral limb movements, motor areas also appear to play a role in ipsilateral limb movements (Matsunami and Hamada, 1981; Tanji et al., 1988; Rao et al., 1993; Donchin et al., 1998; Cisek et al., 2003; Verstynen et al., 2005; Wisneski et al., 2008; Brus-Ramer et al., 2009). Several studies in monkeys have shown that individual M1 neurons, on average, are modulated by ipsilateral arm movements (Donchin et al., 1998; Cisek et al., 2003). Numerous studies have also presented evidence that, after unilateral damage, the 'contralesional' intact hemisphere plays an increased role in ipsilateral movements (Brinkman and Kuypers, 1973; Dancause, 2006; Hummel and Cohen, 2006). Indeed, studies have demonstrated increased activity in homologous regions of the intact hemisphere in stroke patients (Blasi et al., 2002). However, the intact contralesional hemisphere may also play a maladaptive role under certain conditions (Dancause, 2006; Hummel and Cohen, 2006).

To better understand the bihemispheric control of movements, it remains important to understand the distributed neurophysiological representation of ipsilateral limb control. Recent advances in recording technology and computational processing have led to greater characterization of information encoded by simultaneously recorded neural ensembles (Wessberg et al., 2000; Carmena et al., 2003; Mulliken et al., 2008). These efforts have increasingly highlighted differences in the encoding of information at the ensemble level relative to that for single neurons (Wessberg et al., 2000; Averbeck et al., 2006; Mulliken et al., 2008). Here we characterize the distributed ensemble representation of ipsilateral kinematics in both monkey and man using linear regression methods.

We further tested the generality of such a finding by decoding ipsilateral kinematics from cortical field potentials (i.e. local field potential (LFP) in monkeys and subdural electrocorticogram (ECoG) in human subjects). Past work has demonstrated that both LFP (in monkey) and ECoG (in man) can be used to decode direction of contralateral limb movements (Mehring et al., 2003; Schalk et al., 2007). Less is known about continuous decoding of ipsilateral movement parameters from cortical field potentials. While two recent studies demonstrated that ipsilateral limb movements can result in specific patterns of activity (Rickert et al., 2005; Wisneski et al., 2008), it remains unclear if cortical potentials can continuously represent ipsilateral kinematics.

Reliable, continuous decoding of movement parameters represents an important step towards the creation of fully-functional biomimetic Brain-Machine Interfaces (BMI) (Wessberg et al., 2000; Serruya et al., 2002; Taylor et al., 2002; Carmena et al., 2003; Schalk et al., 2007; Mulliken et al., 2008; Schalk et al., 2008). While the majority of studies supporting the development of BMIs have incorporated the contralateral neural representation of movements, there is increasing interest in designing BMIs compatible with extensive hemispheric injury (Buch et al., 2008; Wisneski et al., 2008). Ipsilateral

control would allow a large cadre of patients with motor cortex damage and contralateral weakness to eventually benefit from BMIs. In this study, we also demonstrate that the ipsilateral neural representation can be used in a closed- loop BMI.

4.2 Methods

4.2.1 Monkeys

Surgery. Two adult male rhesus monkeys (*Macaca mulatta*) were chronically implanted in the brain with arrays of 64 teflon-coated tungsten microelectrodes (35 micrometers in diameter, 500 micrometers separation between microwires) in an 8x8 array configuration (CD Neural Engineering, Durham, NC). Monkey P was implanted in the arm area of primary motor cortex (M1) and the arm area of dorsal premotor cortex (PMd), both in the left hemisphere, and the arm area of M1 of the right hemisphere, with a total number of 192 microwires across 3 implants. Monkey R was implanted bilaterally in the arm area of M1 and PMd (256 microwires across 4 implants). Localization of target areas was performed using stereotactic coordinates from a neuroanatomical atlas of the rhesus brain l, 2000). All procedures were conducted in compliance with the National Institutes of Health Guide for the Care and Use of Laboratory Animals and were approved by the University of California at Berkeley Institutional Animal Care and Use Committee.

Electrophysiology. Unit activity was recorded using the MAP system (Plexon Inc, Dallas, TX). For this study, only units from each primary motor cortex were used. Only units that had a clearly identified waveform with a signal-to-noise ratio of at least 4:1 were used. Activity was sorted using an on-line sorting application (Plexon Inc, Dallas, TX) prior to recording sessions. Isolation of units was then verified offline. Large populations of well isolated units were recorded during each daily session in both monkeys.

Electromyography (EMG). Surface gold disc electrodes (Grass Technologies, Inc) were mounted on medical adhesive tape and placed on the skin overlying muscle groups at the beginning of select sessions. Bilateral muscle groups tested included pectoralis major, biceps, deltoid, triceps, trapezius, latissimus dorsi, neck muscles and forearm muscles. EMG signals were amplified by a 10,000 factor with a multi-channel differential amplifier (Grass Technologies, Inc) and stored (Plexon Inc, Dallas, TX). Signals were then high-pass filtered, rectified, and smoothed by convolution with a 25 millisecond triangular kernel, and normalized. Directional activation of each EMG signal was estimated by measuring the activity in a 300 ms window after the onset of movement to each target. EMG signals were collected over ~10 trials in each direction. The significance of this effect was assessed using analysis of variance (ANOVA).

Experimental Setup and Behavioral Training. Monkeys were trained to perform a center-out delayed reaching task using a Kinarm (BKIN Technologies, Kingston, ON) exoskeleton (Figure 13 A). During training and recording, animals sat in a primate chair that permitted limb movements and postural adjustments. Head restraint consisted of the animal's headpost fixated to the chair. Kinematic variables (position, velocity and acceleration) were continuously monitored and recorded.

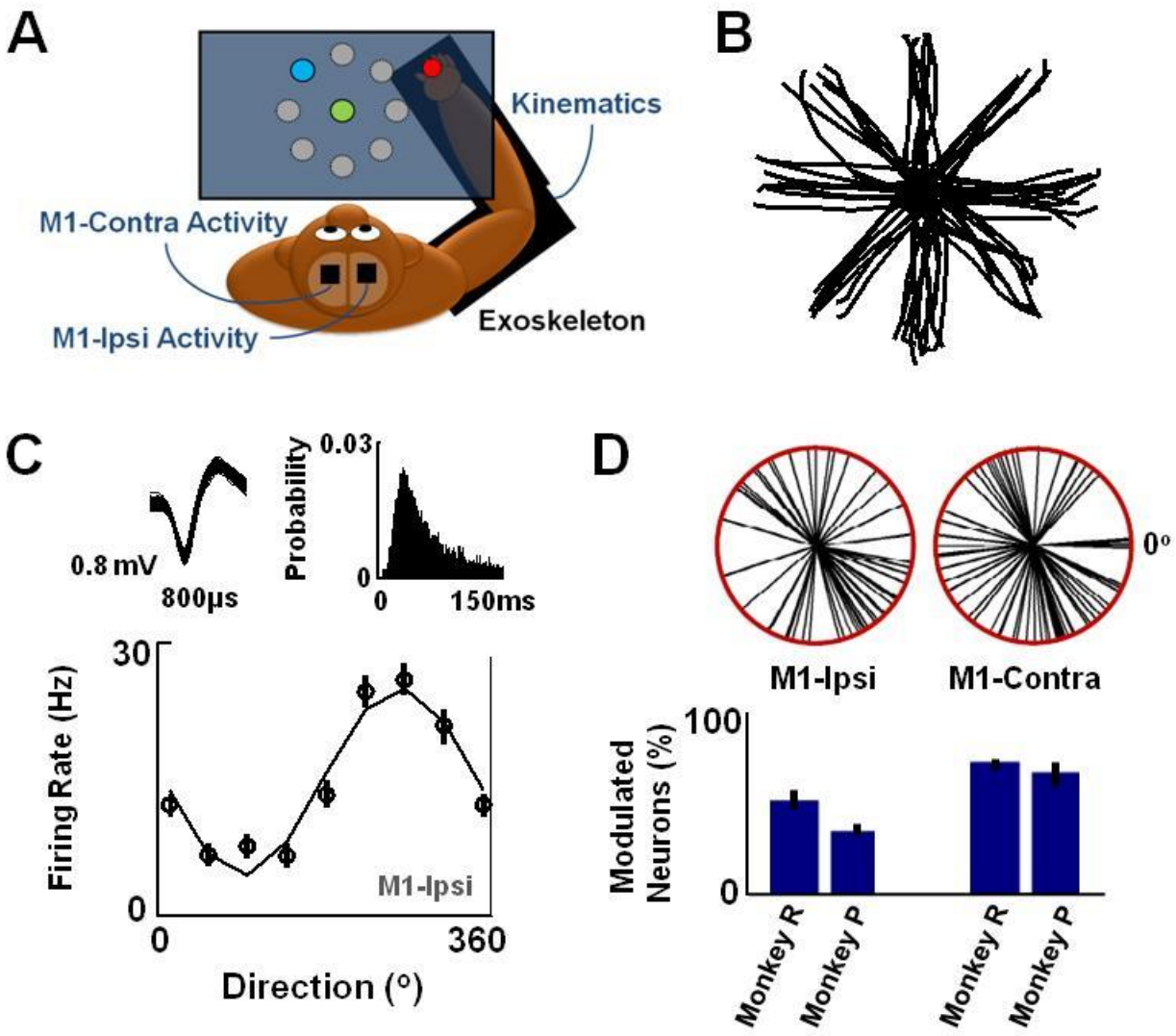

Figure 13 : Directional modulation of bihemispheric M1 unit activity. A, Schematic of the experimental setup for recoding spike and LFP activity from both the ipsilateral and contralateral M1 during the performance of a center-out reaching task with the right upper limb. B, Hand trajectories during performance of the center-out task. C, Directional modulation of the firing rate of a single neuron. Panels above respectively show 150 randomly selected waveform traces and the interspike-interval distribution. Solid line is the cosine fit for directional modulation. Error bars are the SEM. D, Fraction of units from each hemisphere that were significantly modulated. Error bars are the SEM. Circles above show the distribution of preferred directions from Monkey R.

The behavioral task consisted of hand movements from a center target to one of eight peripheral targets (i.e. 'center-out' task) distributed over an ~8cm diameter circle. The workspace was created to minimize any requirement for postural changes during task performance. Target radius was typically 0.75 cm. Trials were initiated by entering the center target and holding for a variable time period of 500-1000ms. The GO cue (center changed color) was provided after the hold period. A liquid reward was provided after a successful reach to each target and a peripheral hold period (200-500ms). Visual feedback

of hand position was provided by a cursor precisely co-located with the center of the hand (radius 0.5cm). During the task, the non-task arm was immobilized in a padded splint.

Decoding motor parameters from neural ensembles. A linear regression model was used to predict limb position and velocity (both joint position and endpoint position). In this model (Equation 1), the inputs, X*(t)*, were a matrix with each column corresponding to the discharges of individual neurons, and each row representing one time bin. The output Y(t), was a matrix with one column per motor parameter. The linear relationship between neuronal discharges in X(t), and behavior in Y(t) was expressed as

$$\mathbf{Y}(t) = \mathbf{b} + \sum_{u=-m}^{n} \mathbf{a}(u)\mathbf{X}(t-u) + \varepsilon(t), \qquad (1)$$

where a and b are constants, calculated to fit the model optimally; a(u) are the impulse response functions required for fitting X(t) to Y(t) as a function of time lag u between inputs and the outputs. Ten time lags were used during these experiments. Second, b represents the Y-intercept in the regression. The final term in the equation, $\varepsilon(t)$, represents residual errors.

Brain-Machine Interface. We used the linear filter described in the previous section to predict shoulder and elbow joint angles from the recorded neural activity (only M1-ipsi activity was included). The model was trained on 10 minutes of activity and then used to predict position from subsequent neural activity (Wessberg and Nicolelis, 2004). Neural activity was streamed over a local intranet via the PLEXNET client-server application (Plexon Inc, Dallas, TX) and converted into 100 ms bins of spiking activity. Each binned value was used to generate real-time predictions of the shoulder and elbow joint angles that were streamed to the Kinarm interface as control signals. The cursor position was updated on the Kinarm projection screen at 10 Hz.

Filter parameters were not changed during each daily Brain Control (BC) experiments (usually 2-3 hours per day). For the multiple experiments reported in Figure 17, the need for daily retraining of the filter (i.e. at the start of a BC session) was determined by the stability of the units. The stability of a recorded unit was solely determined by visually comparing the waveform shape with the previous day's stored template. When all units were putatively stable, no retraining of the filter was performed. If there were any changes in the waveform (e.g. a single waveform change), then the filter was retrained during a manual control session. The animals were then allowed a period of time to relearn the decoder properties (typically ~ 1 hour). Task performance in BC was determined after this period of learning. After this defined period, all subsequent trials and attempts were included in the analysis of task performance (also see below).

4.2.2 Data analysis

Tasks Performance Analysis: A correct trial was defined as successful movement of the cursor to the target. We minimized the number of false-positive self-initiations (i.e. the number of trial attempts by adjusting the required hold period). This threshold was determined by measurements of false triggers when the BMI was engaged but the screen

was turned off (i.e. in the absence of volitional control of the cursor). The time-to-target measurement reflected the movement time from the center to each peripheral target. An error trial consisted of inability to reach the target in 10s.

Predictive power of the decoder: The predictive power of each decoder was determined by comparison (i.e. correlation) of neural predictions of shoulder and elbow angular position with that of measured values. Estimation of predictive power was performed using 2 minutes of movements outside of the 10 minute training window.

Preferred Direction: The significance of the directional modulation of a unit's firing rate was determined using an ANOVA test. Directional tuning was estimated by comparing the mean firing rate as a function of target angle during execution of the movement. The tuning curve was estimated by fitting the firing rate with a sine and a cosine as:

$$f = [B_1\ B_2\ B_3] \times \begin{bmatrix} \text{const} \\ \sin\theta \\ \cos\theta \end{bmatrix} \quad (2),$$

where θ corresponds to reach angle and f corresponds to the firing rate across the different angles (Georgopoulos et al., 1986). Linear regression was used to estimate the B coefficients. The PD was calculated using the following: PD = $\tan^{-1}(B_2/B_3)$, resolved to the correct quadrant.

LFP Analysis: Performed similarly to that outlined below for the electrocorticographic analysis.

4.2.3 Human Subjects

Three subjects (age range 18–35 years) with refractory epilepsy were recruited from a pool of patients undergoing intracranial monitoring for the localization of an epileptogenic focus. Each patient had undergone a craniotomy for chronic (1-2 weeks) implantation of a subdural electrode array and/or depth electrodes. Electrode placement was solely determined on clinical grounds and varied between subjects (Figure 17). Subject 1 was right handed with a left hemispheric grid, subject 2 was left handed with bilateral strips, and subject 3 was left handed with right hemispheric grid. None of the subjects had overt cognitive deficits and antiepileptic drug therapy was discontinued during ECoG recordings. Consenting patients participated in the research study during the week of ECoG monitoring. The study protocol, approved by the UC San Francisco and UC Berkeley Committees on Human Research, did not interfere with the ECoG recording made for clinical purposes, and presented minimal risk to the participating subjects.

Recordings. The electrode grids used to record ECoG signals for this study were either 64-channel 8 × 8 (patient 1, 2, 4, 5) or 4 strips of 8x1 (patient 3) platinum–iridium electrodes. Electrode diameter was 4 mm (2.3 mm exposed), with 10 mm center-to-center spacing. Signals from the ECoG grids were split and sent to both the clinical system and a custom recording system. A broadband (~50 kHz), 256 channels preamplifiers (PZ2-256 256-Channel PreAmp, Tucker-Davis Technologies, Inc) was used to amplify the ECoG signals

with the electrode furthest from the motor cortex used as a reference for all other grid electrodes. The amplified data was then sent to an ultra high performance data acquisition processor over a fast fiber optic connection (RZ2 Z-Series Base Station, Tucker-Davis Technologies, Inc) that digitized the signal at 3052 Hz with 16-bit resolution.

Subjects used a stylus to perform arm movements on the touch-screen connected to designated laptop. The stylus position was registered as a mouse position and was sampled using custom-made MATLAB software. A PC-based, bus-powered USB device (Measurement Computing's USB-1208FS) was used to convert the mouse position to an analog voltage (1-4 V) and these voltages were sent to the analog input of the data acquisition processor (RZ2 Z-Series Base Station, Tucker-Davis Technologies, Inc) to be sampled and stored together with the ECoG signals. During the performance of the task additional event markers (e.g. beginning of a trial, appearance of a target, Acquiring of a target, etc.) were sent to other analog inputs of the data acquisition processor from the digital ports of the PC-based bus-powered USB analog to digital converter (Measurement Computing's USB-1208FS).

Behavioral task. During the recording, subjects were seated in a hospital bed with a touch-screen (KEYTEC INC.) placed in front of them in the horizontal plane. They were asked to use a stylus to perform arm movements on the touch screen using their shoulder and elbow rather than their wrist. To evaluate the coupling between the ipsilateral and contralateral ECoG activity to arm movements we asked each subject to perform the task once with their right hand and one with their left. A trial began with the appearance of a rectangular target (1 cm side) at the center of the reach field. This cue indicated to subjects to move their hand while holding a stylus towards the target; once the center target was obtained, one of several (6 or 8) randomly chosen peripheral targets (1 cm radius) appeared on the touch screen. After the 400±200 msec delay, the center target disappeared. This was the "GO" signal indicating that the subject should perform a reach towards the lit target. Once the target was hit, a new trial began by the appearance of a rectangular target at the center of the reach field. Each subject made 30 reaches to each target (total of 180 or 240 reaches).

Movement reconstruction. The first step in our analysis included filtering, re-referencing, and down-sampling of the ECoG and movement signals. Line noise (60Hz and its harmonics) was removed using a notch filter and then re-referenced by subtracting the common average reference (CAR) from the data of each electrode. CAR was calculated by averaging the raw signal of all the electrodes, omitting the ones that visual inspection suggested poor signal quality. After the re-referencing, the data was band passed between 1 and 250 Hz and down-sampled to 500 Hz.

In order to reconstruct a subject's movements (X and Y position) from the ECoG data, we used the ECoG activity as an input to the Wiener filter. ECoG signals were band-passed into 9 frequency bands (1-8, 9-15, 16-30, 31-50, 51-70, 71-90, 91-110, 111-131, 131-150), followed by calculating the analytic amplitude of each frequency band using the Hilbert transform. The resulting 9 time series were appended to the original time series of the ECoG signal (i.e. a total of 64x10=640 ECoG 'channels' in Subjects 1 and 2). The time series were down-sampled to 15Hz, and 1 second of ECoG data (15 bins) preceding a given point

in time was used to train the model and generate predictions. First, we tested the contribution of each individual new time-series to the prediction of the hand movements and then selected the ones that produced the best prediction to be used as the inputs to the Wiener filter. Estimation of predictive power was always performed using 60 sec of movements outside of the training window and the predictive power of each decoder was determined by comparison of neural predictions of X and Y position with that of measured values.

Statistical analysis. In order to test the statistical significance of our results, we compared correlation-coefficient (CC) distributions for actual and a 'randomly-shifted' version of the same data. To obtain CC distributions for the actual runs, we circularly shifted (MATLAB function circshift) both the ECoG and movement data with a random shift (300 times). We found the best Wiener filter weights for the first 4 minutes of the shifted data and then applied them to the remaining portion. This process resulted in a distribution of CC's for each movement parameter (the means and standard-deviations for the ipsilateral trials are depicted in Table 1). For the 'random-shift' method, we created a distribution by picking a random lag between the movement and the ECoG data (300 times). This time, however, while we shifted the ECoG data, the movement data was held constant. The result of this procedure was another distribution of CC's.

Neural Signal	Elbow	Shoulder	Hand (X)	Hand (Y)
Spikes (n=10)	0.81 ± 0.03	0.78 ± 0.05	0.61 ± 0.04	0.75 ± 0.04
LFP (n=8)	0.47 ± 0.02	0.42 ± 0.02	0.29 ± 0.05	0.45 ± 0.02
ECoG (n=3)	-	-	0.60 ± 0.03	0.61 ± 0.03

Table 1 : Prediction of Ipsilateral Limb Position. Values indicate the correlation coefficient R (mean ± sem). The value of n is the number of sessions used in the analysis.

4.3 Results

4.3.1 Monkeys

We trained two macaque monkeys to perform a center-out reaching task with the right upper limb using the Kinarm Exoskeleton system. Reaching movements with the proximal arm and hand were limited to two-degrees of freedom (flexion/extension of the elbow and shoulder) in the horizontal plane. A cursor (R=0.5 cm) on the horizontal screen was collocated with hand movements (Figure 13 A). Following chronic implantation of microelectrode arrays into bilateral M1, we recorded the neural activity (both spike and LFP) during the performance of a center-out reaching task (Figure 13 B). We first estimated the percentage of units that were significantly modulated by the direction of arm movements. Figure 13 C illustrates a single unit from ipsilateral M1 (M1-ipsi) whose firing rate was directionally modulated. For both animals, the respective fraction of modulated

neurons for M1-ipsi were 43 ± 5% and 54 ± 6 %, while those for contralateral M1 (M1-contra) were 67 ± 6% and 73 ± 7% (Figure 13 D). These estimates (from our chronic recordings) are in-line with past reports using acute recording methods (Donchin et al., 1998; Cisek et al., 2003).

We next used linear regression techniques to characterize the bihemispheric ensemble representation of movement parameters (Humphrey et al., 1970; Ashe and Georgopoulos, 1994; Wessberg et al., 2000; Carmena et al., 2003). In general, while regression techniques have found that multiple parameters (e.g. target direction, position and velocity) are correlated with activity at the level of single neurons, correlations with velocity appear to be the most prominent (Ashe and Georgopoulos, 1994; Reina et al., 2001; Paninski et al., 2004a; Paninski et al., 2004b). This analysis used neural activity that was closely temporally linked to external movements (i.e. temporal lag of < 100 ms).

We first performed a similar analyses for units recorded from both M1-ipsi and M1-contra. Consistent with past results, we found that individual unit activity in M1-contra was more closely associated with velocity than position (data not shown). For M1-ispi, we also found that individual unit activity was significantly more correlated with velocity than position (position: 0.05 ± 0.03; velocity: 0.16 ± 0.02 mean ± sem; $p < 0.001$ t-test). However, when the same analysis was performed with neural ensembles from each hemisphere (i.e. single bin of 100ms with at least 50 units per hemisphere), both parameters could be decoded equally well (M1-ipsi: 0.50 ± 0.05 and 0.49 ± 0.06 for position and velocity respectively, $p > 0.3$ t-test). Identical results were obtained regardless of whether angular joint or hand-based coordinates were used for comparison of position and velocity predictions. Taken together, this further indicates that information not readily apparent at the single neuron resolution (i.e. velocity more represented than position) can be reliably decoded from neural ensembles (i.e. velocity and position are equally represented).

We next performed an additional set of analysis to directly compare with methods typically used for real-time continuous prediction of movement parameters (Wessberg et al., 2000; Serruya et al., 2002; Carmena et al., 2003). One key difference is the simultaneous inclusion of multiple temporally lagged bins into the regression model (e.g. 10 lags are typically used). While the animals performed center-out reaching movements with the right upper limb, the recorded M1 spike activity (the respective ipsilateral and contralateral spike activity were grouped separately) was correlated with limb kinematics to generate decoders for each variable (Figure 14A). Hence, we will use the term 'decoder' to refer to the combined transforms. Figure 14 B illustrates the predictive ability of either the ipsilateral or the contralateral neural ensemble activity during a single session. For multiple sessions in both monkeys (n=5 sessions each, 10 lags with at least 50 units/hemisphere), ipsilateral ensemble activity could reliably and continuously predict angular joint positions (Table 1). We subsequently generated a "neuron-dropping curve" (Wessberg et al., 2000; Carmena et al., 2003) for each movement parameter to estimate the relationship between ensemble size and the representation of a given parameter. For both subjects, the fidelity of the representation improved as a function of the size of the neural ensemble (Figure 14C).

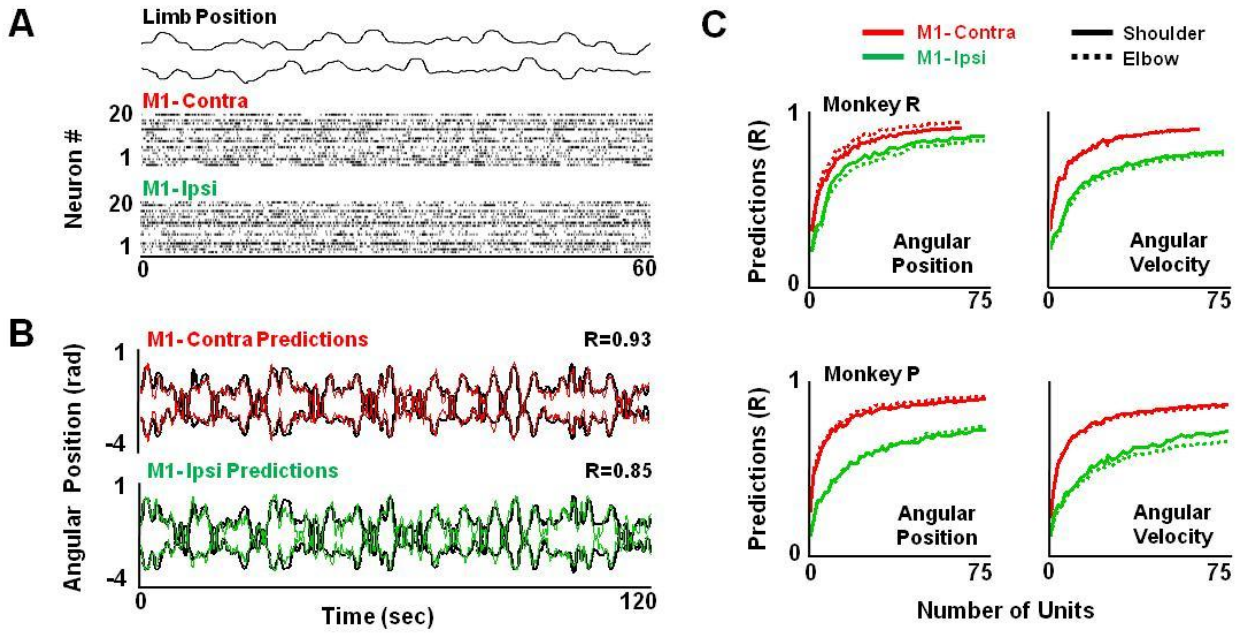

Figure 14: Real- time decoding of ipsilateral upper limb parameters from M1 spike activity. A, Continuous illustration of shoulder (upper) and elbow (lower) angular position and spiking data from each hemisphere. Each dot represents a single spike. B, Predictions of elbow and shoulder position from ensembles of ipsilateral and contralateral spike activity. Dark traces show the movements across time. While the red trace shows the prediction from contralateral M1, the green trace shows that for ipsilateral M1. R is the correlation between the predicted and the actual traces. C, Neuron-dropping curves to illustrate the relationship between ensemble size and predictive ability for both angular position and velocity for Monkey P and R. Dotted line (shoulder), solid line (elbow).

With the simultaneous inclusion of temporally lagged bins from M1-ipsi, limb position could be better decoded than velocity (with 10 lags, R=0.8 ± 0.02 and 0.69 ± 0.04 mean ± sem for position and velocity respectively, $p<0.0001$ t-test). Consistent with this notion was the observation of a relatively sharper decline in velocity-related information for increasing temporally lagged bins (Supplementary figure 4). It is possible that the inherent autocorrelation of changes in limb position or velocity during this task underlies this result (Paninski et al., 2004b). We also assessed the relation between M1-ipsi activity and the coordinate system for estimating limb position (i.e. joint vs hand position). In our experimental system, the robotic exoskeleton allows accurate monitoring of joint angles as well as hand position. In both animals, we consistently found that both the contralateral and ipsilateral ensemble activity were more correlated with angular joint kinematics than end-point hand coordinates ($p < 0.001$, ANOVA, Table 1).

What is the temporal evolution of the predictions from each hemisphere relative to limb movements? We performed high resolution (time bins of 10 ms) analysis of the predictive ability of neural ensembles from each hemisphere. Consistent with past reports, we observed a delayed peak in the relationship between M1-contra activity and limb position (~50ms, Figure 15). In contrast, the value of this relationship was delayed for M1-ipsi (~110 ms). Thus, it appeared that at least a portion of the M1-ipsi neural representation is delayed relative to that from M1-contra.

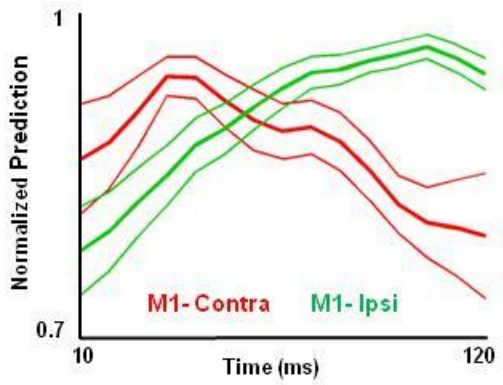

Figure 15: Temporal evolution of upper limb movement parameters. Each curve shows the temporal evolution of the predictive ability of ensemble of neurons from either the contralateral or ipsilateral M1 (mean ± sem). Ensemble predictions of limb position were performed using a single bins of data (10 ms bin size) lagged from the onset of movement (step size=10 ms, non-overlapping). The peak of each curve was normalized to 1 prior to generation of the mean curves shown.

To exclude the possibility that M1-Ipsi activity simply reflected spurious activation of the opposite limb (e.g. postural adjustments or mirror movements with the left hemibody during reaches with the right arm), we measured bilateral EMG activity during select sessions (Cisek et al., 2003). Figure 16 illustrates the directional modulation of the EMG activity for the right biceps and left pectoralis during reaches with the right arm. For Monkey P, there was no evidence of significant activation of the left hemibody during reaching movements. For Monkey R, only one left hemibody muscle (left trapezius) demonstrated significant activation during the task. Together, these results confirmed that M1-Ipsi activity largely did not reflect spurious activation of the opposite hemibody.

We next quantified the ability of cortical field potentials to continuously represent ipsilateral kinematic parameters. We used spectral decomposition of the LFP signal as an input to the Wiener filter (Schalk et al., 2007). The M1-ipsi LFP was also found to be significantly correlated with ipsilateral limb kinematics (Table 1).

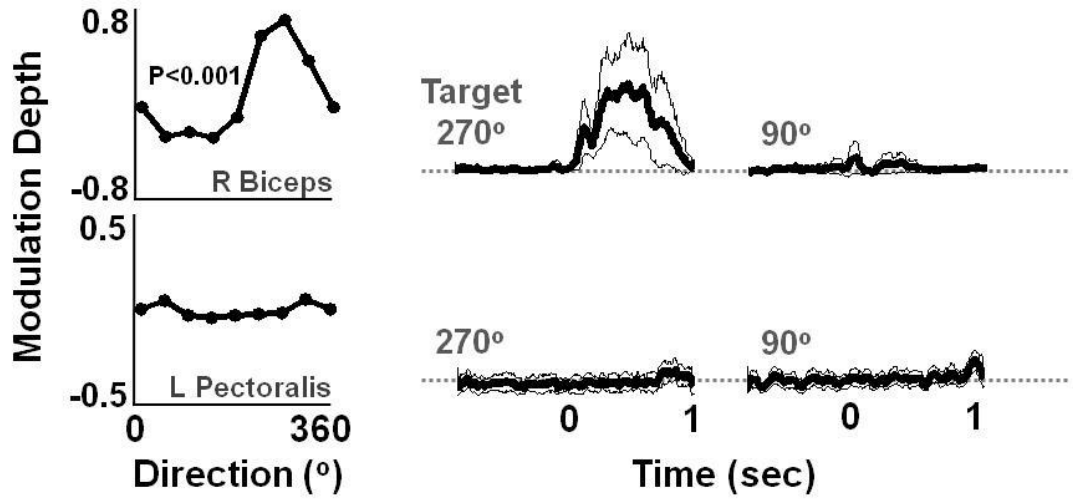

Figure 16 : EMG activity during performance of the center-out task. Representative examples of the directional modulation of the right (R) biceps and the left (L) pectoralis EMG. Each dot represents the mean activity in a 300 ms window after movement onset. Traces on the right show the mean (dark line) ± SEM (thin line) EMG activity to two targets. * (p < 0.001, ANOVA).

4.3.2 Human Subjects

We assessed the generality of our results to primate motor systems by testing this relationship in three human subjects. Electrocorticographic (ECoG) recordings from patients with epilepsy offer a means to evaluate the ability of cortical field potentials to predict ipsilateral motor parameters (Schalk et al., 2007; Schalk et al., 2008). ECoG signals (from either the left or right hemisphere) were recorded from three subjects during the performance of center-out reaches with each hand. Traces of hand movements are depicted in Figure 17 B. Shown in Figure 17 C are representative velocity profiles of the movement from the center to each of the targets.

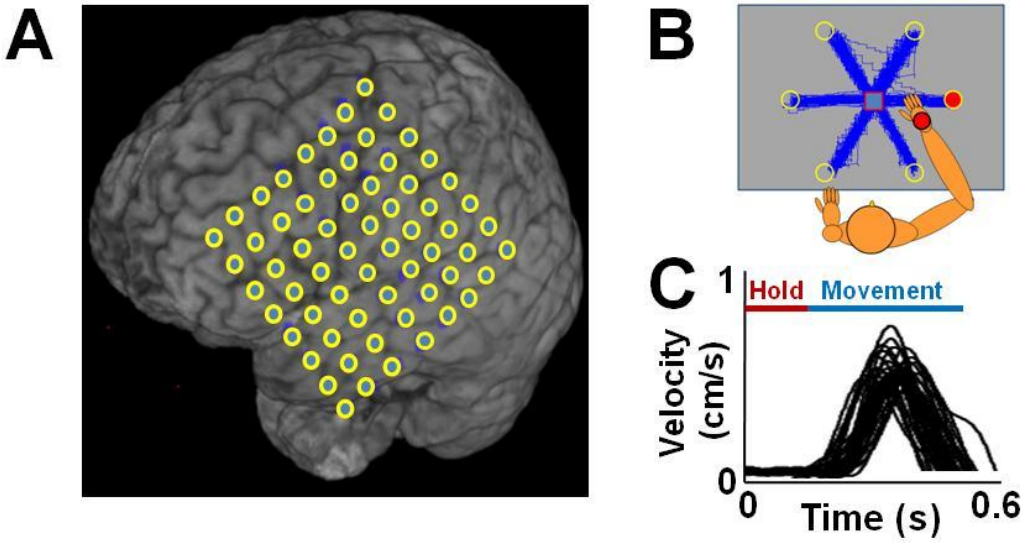

Figure 17 : Experimental setup and task characteristics. A, Electrode placement overlaid on the brain MRI of subject 1. B, Actual hand trajectories during performance of the center-out reaching task. The dimensions of the workspace were 20 x 20 cm. C, Multiple examples of the velocity profiles for movements from the center (i.e. during period marked as 'Hold') to the target. Profiles for all targets are shown in an overlapping manner.

We next evaluated whether linear regression methods could continuously decode ipsilateral upper arm position. A reconstruction of hand trajectories from the recorded neural signals is illustrated in Figure 18A. For three such subjects, cortical field potentials were found to be significantly correlated with ipsilateral limb kinematics (Table 1). In addition, bilateral surface EMG measurements during the performance of this task did not reveal evidence of the opposite hemibody activation.

We also assessed the anatomical distribution of such predictive information. While this was observed to be relatively distributed, activation appeared to be most prominent in sensorimotor regions (Figure 18B and Supplementary figure 5). Shown in Figure 18C are the bands which contributed the most to the prediction of ipsilateral limb movements (also see Supplementary figure 6 for mean of all subjects). Moreover, we attempted to compare

the temporal evolution of predictions for both hemispheres. For cortical field potentials at the level of ECoG, no significant differences could be detected between the two hemispheres.

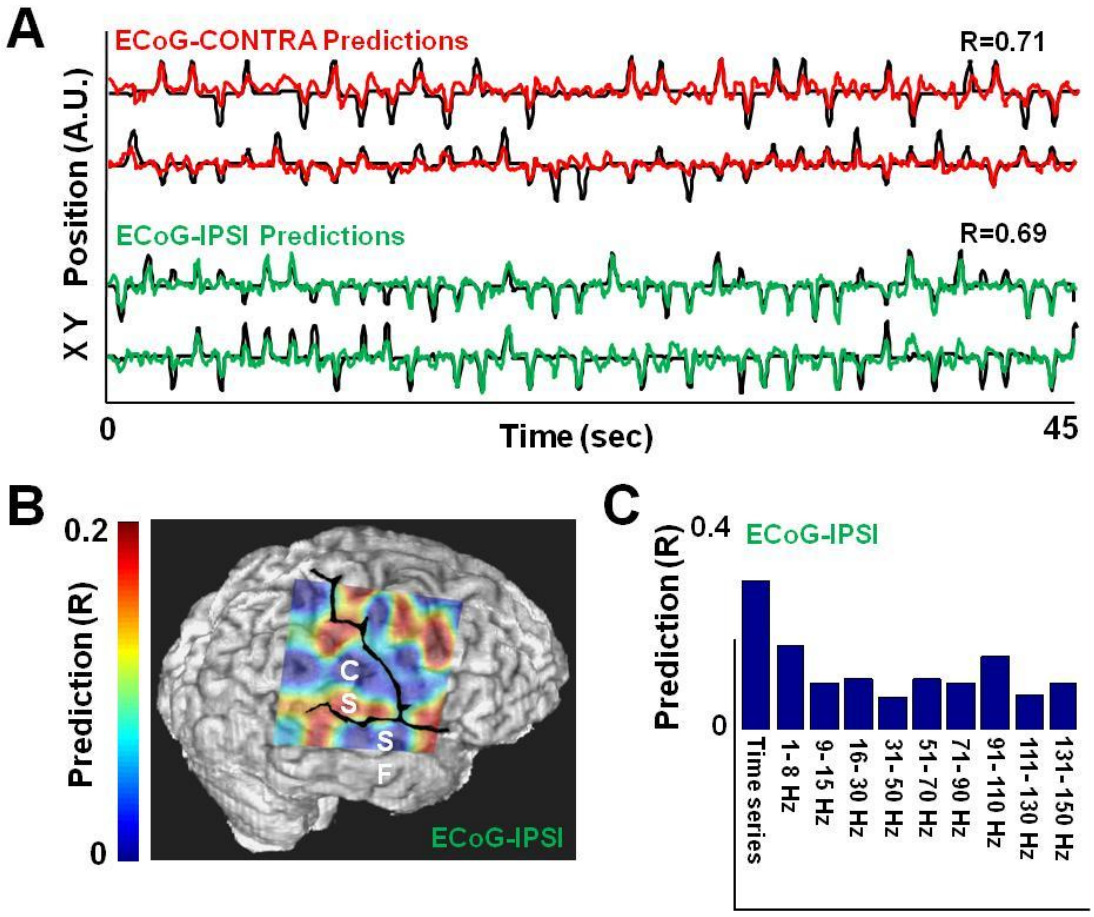

Figure 18: Reconstruction of hand position from ECoG data. A, Prediction of hand position from either the ipsilateral or the contralateral ECoG activity. Dark traces show the actual movements. Red trace shows the prediction of the contralateral hand position; green trace shows that for the ipsilateral hand. R is the correlation between the predicted and the actual traces. B, Colormap illustrating the relationship between the anatomical locations of electrodes and its predictive ability. Superimposed on the brain image is the predictive ability of individual electrodes. CS = central sulcus, SF = Sylvian Fissure. C, Quantification of the relationship between the timeseries or the frequency band and the ability to predict movement parameters. In this analysis, only the information from a single band was included in the model.

4.3.3 Ipsilateral Neural Representation for closed-Loop BMI in Monkeys

The results above indicate that ipsilateral movement parameters can be reliably represented in both M1 spike activity as well as cortical field potentials in both monkey and man. We subsequently asked whether a decoder trained under such conditions can be successfully used in a closed loop BMI in monkeys (Figure 19A). Figure 19B illustrates the typical cursor trajectories under control 'brain-control' (BC, where the neural activity exclusively controlled the position of the computer cursor). After a period of training, each monkey could perform the center-out task in BC. For multiple sessions, both animals could accurately perform the center-out task in BC (Monkey P: 83 ± 6% accuracy with a mean

time to reach the target of 2.4 ± 0.5 s; Monkey R: 76 ± 9 % accuracy with a mean time to reach the target of 2.9 ± 0.3s; all reported as mean ± sem).

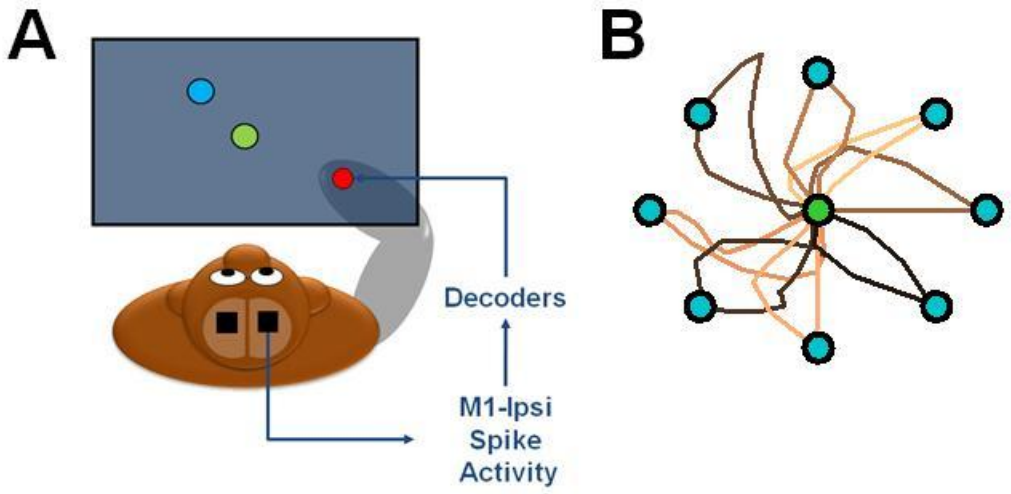

Figure 19: Closed-loop BMI using the ipsilateral neural representation of arm movements. A, Schematic illustrating cursor control by M1-ipsi. B, Representative traces of the cursor movement from the center to each of the eight targets and back.

4.4 Discussion

Our results demonstrate that the distributed activity in primate motor areas can reliably and continuously represent ipsilateral upper limb kinematics. We found that such information could be decoded by applying linear methods to neural signals at a variety of temporal and spatial scales (ensemble spike activity as well as the aggregate cortical field potential at two different resolutions). We further demonstrate that the spike activity from M1 can be used in a biomimetic closed-loop BMI designed to control ipsilateral limb kinematics.

Role of Motor Cortex in Ipsilateral Movements

Several studies have demonstrated that the activity of single M1 neurons can be modulated by ipsilateral arm, hand and finger movements (Tanji et al., 1988; Donchin et al., 1998; Cisek et al., 2003). Studies in monkeys have further shown that while subsets of M1 neurons are exclusively tuned to the direction of ipsilateral arm movements, another fraction of neurons are active during bimanual movements (Donchin et al., 1998). Lesion and stimulation studies in both monkey and man provide additional support for a role of motor regions in ipsilateral limb control (Brinkman and Kuypers, 1973; Rao et al., 1993; Verstynen et al., 2005; Dancause, 2006; Brus-Ramer et al., 2009).

We demonstrate that ipsilateral limb kinematics can be reliably decoded, in real-time, from the population activity at multiple scales in motor areas. However, the exact role of motor cortex in the control of ipsilateral proximal and distal limb movements remains unclear. The anatomical substrate for the control of ipsilateral movements has been hypothesized to be mediated through either descending uncrossed fibers or trancallosal pathways

(Dancause, 2006). Our finding that the peak of ipsilateral movement prediction is delayed relative to that for contralateral movements lends some support to the notion of interhemispheric transfer of this representation.

One focus of this study was to characterize the representation of arm and hand movement parameters in ipsilateral neural ensembles. Our finding that both the ensemble spiking activity and the population cortical field potentials obtained at two temporal and spatial resolutions can continuously predict ipsilateral limb kinematics further demonstrates that distributed neural ensembles can reliably encode information. Coordinated and dexterous bimanual movements likely require a high-fidelity representation of ipsilateral kinematics. One possibility is that it is an efference copy of contralateral motor commands. Another possibility is that it mediates bimanual coupling (Donchin et al., 1998). Thus, it could provide a neural substrate for the observed phenomenon of spatial coupling during bimanual tasks (Oliveri et al., 2001).

An interesting observation was that M1 activity was more indicative of joint position than hand kinematics (Table 1). Past analysis of the contralateral representation of limb movements have shown that it is correlated with multiple movement parameters (Ashe and Georgopoulos, 1994; Reina et al., 2001; Paninski et al., 2004a; Paninski et al., 2004b). However, because hand position covaries with joint angles and other aspects of arm movement it remains difficult to conclude what is truly encoded in these neurons (Reina et al., 2001). Moreover, it remains possible that a generative model could provide a more parsimonious explanation for the apparent encoding of multiple parameters (Todorov, 2000). It is less clear how to formulate such a model (e.g. direct control of musculature) for the ipsilateral neural representation.

It is also important to note that an alternate explanation for the apparent modulation of neural activity by ipsilateral movements is that the opposite non-task arm and the axial musculature may be active (Cisek et al., 2003). There are at least two lines of evidence suggesting that this does not exclusively account for all neural activity putatively related to ipsilateral limb movements. Classical studies demonstrated that proximal arm movements can be exclusively controlled by ipsilateral motor cortex (Brinkman and Kuypers, 1973). Moreover, distal limb movements made in the absence of proximal movements resulted in ipsilateral neural activity (Tanji et al., 1988). In this study, we minimized the need for postural adjustments. The workspace was optimized such that reciprocal postural movements were not obviously required. While one monkey was found to have limited spurious non-task arm EMG activity, the other did not. Moreover, the task performed by the human subjects did not appear to result in such spurious activity. While it remains difficult to completely exclude that a component of neural activity was related to non-task arm activity, it seems unlikely to account for our observations.

Possible role of the ipsilateral representation in neurorehabilitation

The exact role of ipsilateral motor regions in the recovery of arm function after brain injury remains unclear. There is a significant fraction of patients who do not recover function after a stroke (Dancause, 2006; Hummel and Cohen, 2006). Large subcortical strokes (i.e. with loss of descending contralateral corticospinal pathways) are associated with such a

lack of functional recovery (Shelton and Reding, 2001). This further suggests that ipsilateral motor areas and its associated descending connections are not sufficient by themselves to support recovery. In contrast, in patients who experience spontaneous recovery of limb function, the ipsilateral hemisphere may play a greater role (Gerloff et al., 2006; Lotze et al., 2006). Trancallosal pathways have been implicated in this process (Dancause, 2006; Gerloff et al., 2006). Thus, a likely possibility is that in the presence of the appropriate anatomical substrate, ipsilateral motor areas may assist the process of functional recovery.

Importantly, there is also evidence that the contralesional hemisphere (i.e. ipsilateral to the affected limb) can play a maladaptive role in stroke patients (Dancause, 2006; Hummel and Cohen, 2006). For instance, inhibition of the contralesional hemisphere through non-invasive methods can transiently improve motor function (Hummel and Cohen, 2006). Thus, the ipsilateral hemisphere appears to dampen the excitability of the damaged hemisphere and impede the process of recovery. These studies indicate that the balance of interhemispheric inhibition is important. In this context, another interpretation of our findings is that it represents the transcallosal shaping of ipsilateral motor areas. In the damaged brain, this may impede recovery. Future research may help to uncover how the ipsilateral hemisphere can either facilitate or impede recovery.

A BMI using the Neural Representation of the Ipsilateral Arm

Our results demonstrate that the ensemble representation of ipsilateral arm movements can be used in a closed-loop biomimetic BMI. Past work has not shown that such a representation can be exclusively used to create a closed-loop biomimetic BMI. The decoder used in these experiments predicted the natural relationship between M1 spike activity and ipsilateral movements. It is likely that neurons more sensitive to ipsilateral arm movements than to contralateral arm movements needed to be actively modulated during BC. As in past studies, feedback and learning during closed-loop control were important for improvements in task performance over the course of a session (Taylor et al., 2002; Carmena et al., 2003; Hochberg et al., 2006; Mulliken et al., 2008).

Past work has suggested that the accuracy of movement parameter decoding (Wessberg et al., 2000) is important for BMI function (Taylor et al., 2002; Carmena et al., 2003; Schalk et al., 2007). Linear algorithms have been demonstrated to be reliable in extracting parameters from simultaneously recorded neural activity (Wessberg et al., 2000; Carmena et al., 2003; Mulliken et al., 2008). There is mixed evidence regarding the magnitude of improvements with more sophisticated decoding techniques (Kim et al., 2006; Wu et al., 2006; Mulliken et al., 2008). Most importantly, however, our results indicate that even while the ipsilateral predictions are not as good as the contralateral predications, they can be successfully incorporated in a BMI.

An important question for future research is to fully understand the role of biomimetic decoders (Radhakrishnan et al., 2008). Recent work has suggested that a combination of volitional control of neural activity, visual feedback and plasticity mechanisms can allow direct neural control of neuroprosthetic devices independent of any relationship to natural movements (Moritz et al., 2008; Ganguly et al., 2009). However, given that cortical

networks in M1 are likely optimized for dexterous bimanual limb control, a seemingly likely possibility is that biomimetic decoders can best capitalize upon existing cortical architecture. For instance, comparison of both unimanual and bimanual movements has revealed that both overlapping and non-overlapping patterns of activity are present (Donchin et al., 1998; Wisneski et al., 2008). Accordingly, it remains possible that integration of a biomimetic decoder for ipsilateral movements will not interfere with existing cortical networks for contralateral movements. Such interference could occur if neurons were incorporated into a BMI without regard for their actual relationship to natural movements.

A BMI for patients with chronic stroke

A recent study demonstrated that volitional control of non-invasively recorded neural signals (with MEG) is possible even in chronic stroke patients with limb paralysis (Buch et al., 2008). While arm function did not improve outside of training sessions, subjects could control a prosthetic device through modulation of the μ-rhythm. Interestingly, they could utilize μ-rhythms from either ipsilateral or contralateral brain regions.

In general, the resolution of recorded neural signals (e.g. non-invasive versus invasive intracortical recordings) required for a long-term, reliable BMI remains unclear. Thus, continued basic and translational research using a variety of neural signals is important. Our study explores the eventual creation of an invasive biomimetic BMI based on the ipsilateral neural representation of arm movements. We characterized the ipsilateral ensemble representation of continuous limb movements in non-paralyzed subjects. Methodological limitations (i.e. recording technique and size of cortical area monitored) prevent detailed comparison of the ipsilateral representation in non-human and human subjects. However, it is reassuring that qualitatively similar results were obtained in both healthy non-human primates as well as in patients with chronic focal epilepsy with unclear long-term effects on cortical organization. It will be important to demonstrate that this representation is intact after damage to the opposite brain hemisphere. In support of this concept are imaging studies demonstrating that even after extensive damage to contralateral motor areas, contralesional motor areas are active in a similar manner (Dancause, 2006; Buch et al., 2008).

4.4.1 Conclusion

In summary, our results provide evidence that motor areas encode ipsilateral limb kinematics with high precision. Moreover, this representation can be used in a closed-loop BMI. These findings suggest the possibility of eventually creating fully functional BMIs for patients suffering from extensive unilateral hemisphere brain injury.

5 Appendix I : Supplementary Figures

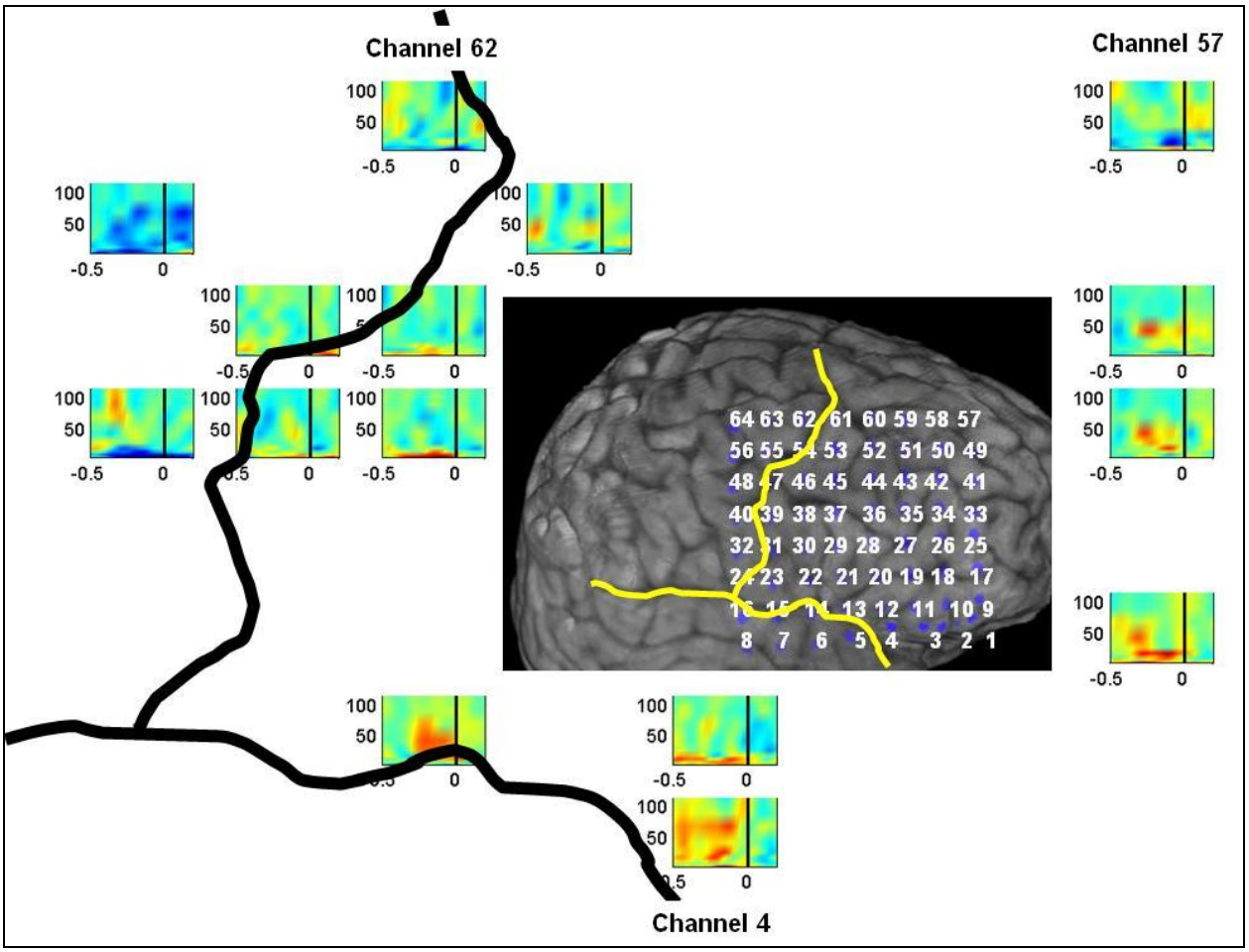

Supplementary figure 1: Event-related time–frequency plots in response to non direction specific movement onset (subject 1). The location of the electrodes with the electrode number is depicted in the MR scan. X axis of each ERSP is time (0.5sec till 0.2 after prior to movement onset, vertical lines at t=0 indicate movement onset), Y axis are the frequency bands (see methods), color code represent z-score values based on permutation analysis (see methods). Electrodes with activations below significance threshold (t-test alpha=0.001, p=0.0001 multi-comparison corrected) are omitted

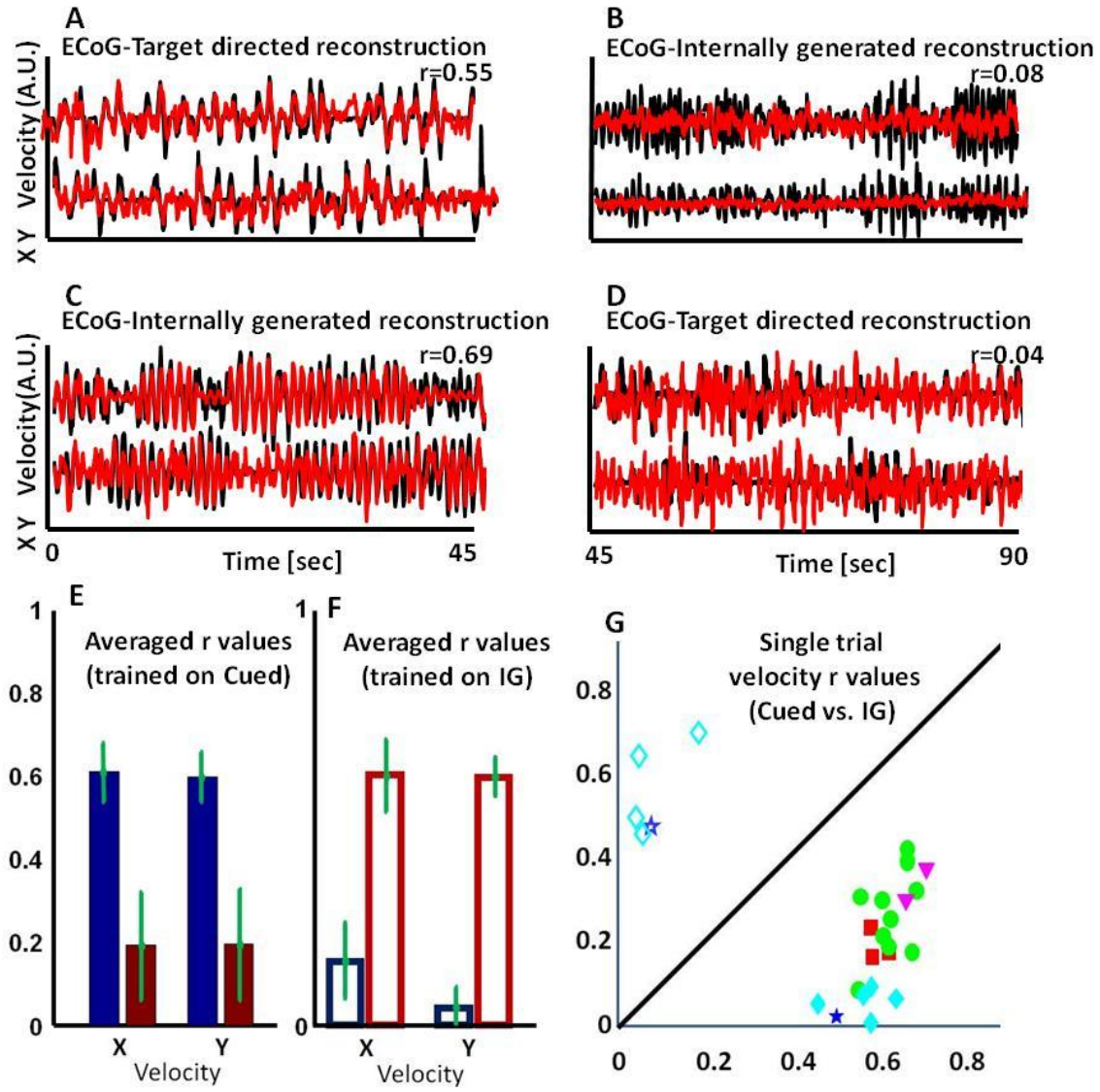

Supplementary figure 2: Comparison of observed and reconstructed hand velocity based on a model derived from ECoG data (A.U. means arbitrary units). Upper row: Model with externally-cued condition as training set used to reconstruct hand velocity for same condition (A) or internally-generated condition (B). Middle row: Model with internally-generated condition as training set used to reconstruct hand velocity for same condition (C) or externally-cued condition (D). The traces and r values are as described in Figure 11. (E-F) Grand average of similarity coefficients between the reconstructed and actual traces. Blue bars: reconstructed externally-cued velocity; Red bars: reconstructed internally-generated velocity. G) Similarity coefficients for the two movement conditions from individual blocks. Solid and empty marks are data points derived by training the model on externally-cued and internally-generated condition respectively. The X value is the r_{SC} for reconstructing externally-cued movement and the Y value is the r_{SC} for reconstructing internally-generated movement. Colors indicate different subjects.

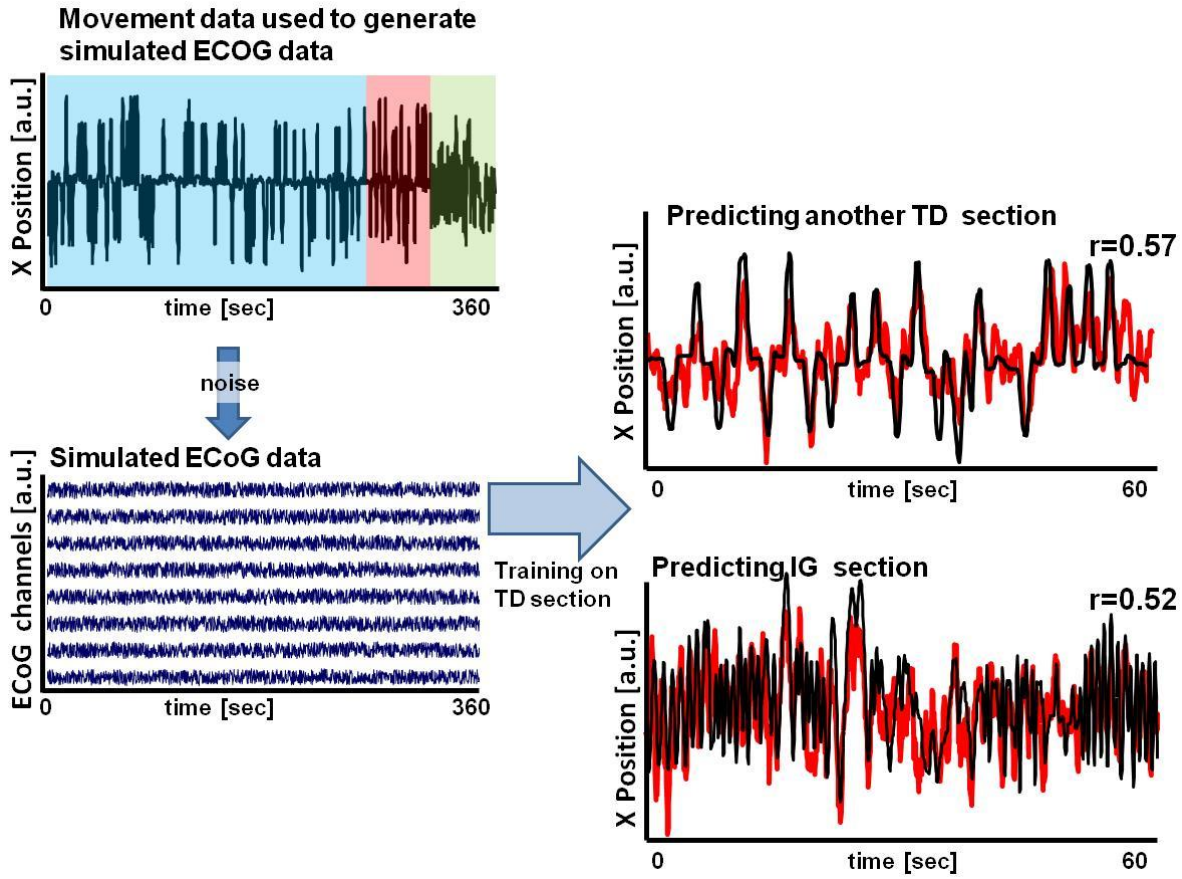

Supplementary figure 3 : Simulated ECoG data using movement data.

Supplementary Figures

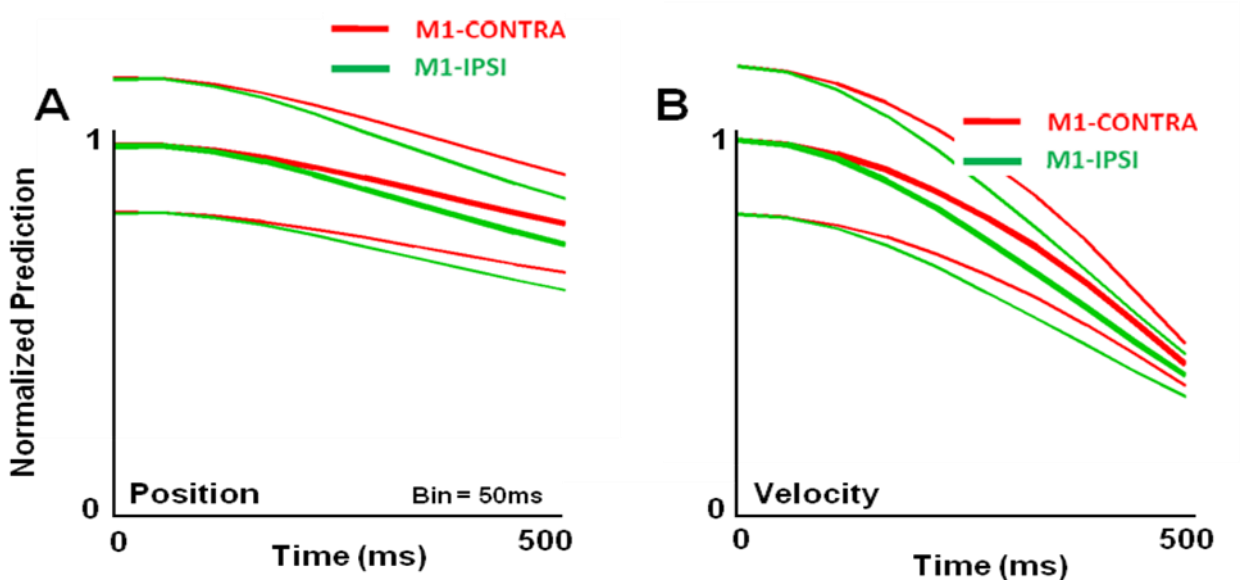

Supplementary figure 4: Comparison of the predictive ability with temporally lagged bins. A, Normalized predictions of limb position using neural activity from a non-overlapping single bin (bin size=50ms, lagged from 0 to 500ms in 50ms steps). Each curve is shown with the mean (thick) ± standard deviation (thin). M1-ipsi (green); M1-contra (red). B, Normalized predictions of limb velocity performed similarly as in A. Note the more rapid decay of predictions of velocity than that for predictions of position.

Supplementary Figures

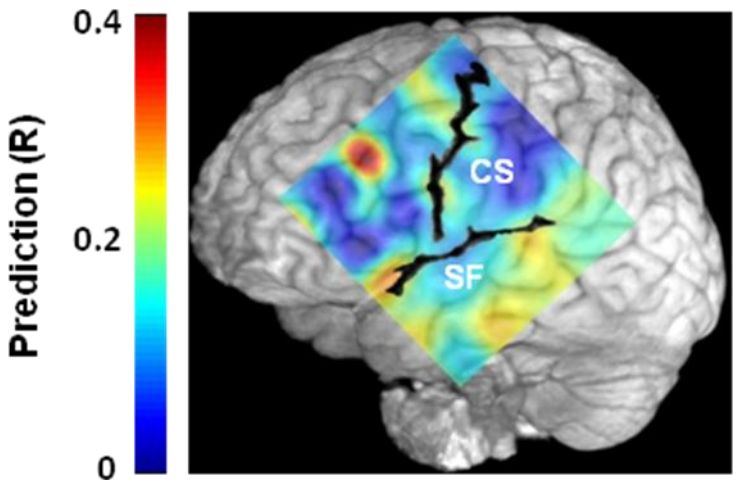

Supplementary figure 5: Anatomical distribution of predictive information. Color map illustrating the relationship between the anatomical locations of electrodes and its predictive ability. Superimposed on the brain image is the predictive ability of individual electrodes. CS = central sulcus, SF = Sylvian Fissure.

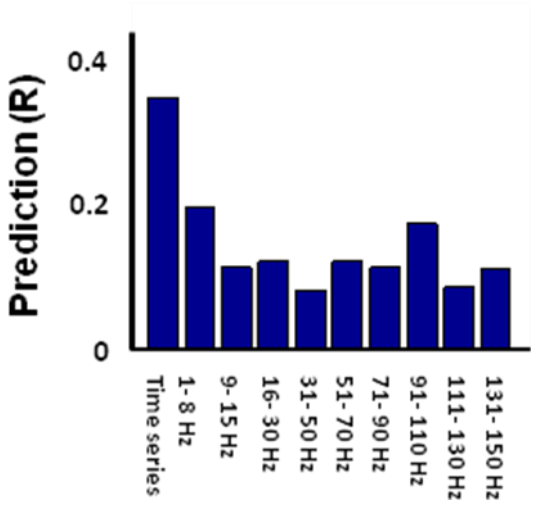

Supplementary figure 6: Quantification of the relationship between the time series or the frequency band and the ability to predict movement parameters. This plot represents the mean from all three subjects.

6 Appendix II: MATLAB codes

6.1 ERP - The full algorithm

```
fftbrainData=fft(brainData);
ffteventData=fft(fliplr(eventData));
newERP=fftshift(ifft(fftbrainData.*ffteventData));
meanSurr=mean(newERP(ceil(length(newERP/2)*rand(1,10000))));
stdSurr =std (newERP(ceil(length(newERP/2)*rand(1,10000))));
 outputERP =(newERP(Tbefore:Tafter)-meanSurr)./stdSurr;
```

6.2 ERSP - The full algorithm

```
for f=1:length(freqs)
        fftbrainData=fft(brainData);
        fftanamp=fft(abs(ifft(fftbrainData*filter(freqs(f)))))
        ffteventData=fft(fliplr(eventData));
        newERP=fftshift(ifft(fftanamp.*ffteventData));
        meanSurr=mean(newERP(ceil(length(newERP/2)*rand(1,10000))));
        stdSurr =std (newERP(ceil(length(newERP/2)*rand(1,10000))));
         outputERSP(f,:) =(newERP(Tbefore:Tafter)-meanSurr)./stdSurr;
end
```

7 References

Aflalo TN, Graziano MS (2006) Partial tuning of motor cortex neurons to final posture in a free-moving paradigm. Proc Natl Acad Sci U S A 103:2909-2914.

Aflalo TN, Graziano MS (2007) Relationship between unconstrained arm movements and single-neuron firing in the macaque motor cortex. J Neurosci 27:2760-2780.

Amador N, Fried I (2004) Single-neuron activity in the human supplementary motor area underlying preparation for action. J Neurosurg 100:250-259.

Amirikian B, Georgopoulos AP (2003) Modular organization of directionally tuned cells in the motor cortex: is there a short-range order? Proc Natl Acad Sci U S A 100:12474-12479.

Aoki F, Fetz EE, Shupe L, Lettich E, Ojemann GA (1999) Increased gamma-range activity in human sensorimotor cortex during performance of visuomotor tasks. Clin Neurophysiol 110:524-537.

Asaad WF, Rainer G, Miller EK (2000) Task-specific neural activity in the primate prefrontal cortex. J Neurophysiol 84:451-459.

Ashe J, Georgopoulos AP (1994) Movement parameters and neural activity in motor cortex and area 5. Cereb Cortex 4:590-600.

Averbeck BB, Latham PE, Pouget A (2006) Neural correlations, population coding and computation. Nat Rev Neurosci 7:358-366.

Baker SN, Kilner JM, Pinches EM, Lemon RN (1999) The role of synchrony and oscillations in the motor output. Exp Brain Res 128:109-117.

Ball T, Schulze-Bonhage A, Aertsen A, Mehring C (2009) Differential representation of arm movement direction in relation to cortical anatomy and function. J Neural Eng 6:016006.

Baraldi P, Porro CA, Serafini M, Pagnoni G, Murari C, Corazza R, Nichelli P (1999) Bilateral representation of sequential finger movements in human cortical areas. Neurosci Lett 269:95-98.

Ben-Shaul Y, Drori R, Asher I, Stark E, Nadasdy Z, Abeles M (2004) Neuronal activity in motor cortical areas reflects the sequential context of movement. J Neurophysiol 91:1748-1762.

Bestmann S, Swayne O, Blankenburg F, Ruff CC, Haggard P, Weiskopf N, Josephs O, Driver J, Rothwell JC, Ward NS (2008) Dorsal premotor cortex exerts state-dependent causal influences on activity in contralateral primary motor and dorsal premotor cortex. Cereb Cortex 18:1281-1291.

Bizzi E, Tresch MC, Saltiel P, d'Avella A (2000) New perspectives on spinal motor systems. Nat Rev Neurosci 1:101-108.

Bizzi E, D'Avella A, Saltiel P, Tresch M (2002) Modular organization of spinal motor systems. Neuroscientist 8:437-442.

Blasi V, Young AC, Tansy AP, Petersen SE, Snyder AZ, Corbetta M (2002) Word retrieval learning modulates right frontal cortex in patients with left frontal damage. Neuron 36:159-170.

Brinkman J, Kuypers HG (1973) Cerebral control of contralateral and ipsilateral arm, hand and finger movements in the split-brain rhesus monkey. Brain 96:653-674.

Brus-Ramer M, Carmel JB, Martin JH (2009) Motor cortex bilateral motor representation depends on subcortical and interhemispheric interactions. J Neurosci 29:6196-6206.

Buch E, Weber C, Cohen LG, Braun C, Dimyan MA, Ard T, Mellinger J, Caria A, Soekadar S, Fourkas A, Birbaumer N (2008) Think to move: a neuromagnetic brain-computer interface (BCI) system for chronic stroke. Stroke 39:910-917.

Canolty RT, Soltani M, Dalal SS, Edwards E, Dronkers NF, Nagarajan SS, Kirsch HE, Barbaro NM, Knight RT (2007) Spatiotemporal dynamics of word processing in the human brain. Front Neurosci 1:185-196.

Carmena JM, Lebedev MA, Crist RE, O'Doherty JE, Santucci DM, Dimitrov DF, Patil PG, Henriquez CS, Nicolelis MA (2003) Learning to control a brain-machine interface for reaching and grasping by primates. PLoS Biol 1:E42.

Catalan MJ, Honda M, Weeks RA, Cohen LG, Hallett M (1998) The functional neuroanatomy of simple and complex sequential finger movements: a PET study. Brain 121 (Pt 2):253-264.

Cheney PD, Fetz EE (1980) Functional classes of primate corticomotoneuronal cells and their relation to active force. J Neurophysiol 44:773-791.

Cisek P, Crammond DJ, Kalaska JF (2003) Neural activity in primary motor and dorsal premotor cortex in reaching tasks with the contralateral versus ipsilateral arm. J Neurophysiol 89:922-942.

Crone NE, Miglioretti DL, Gordon B, Lesser RP (1998a) Functional mapping of human sensorimotor cortex with electrocorticographic spectral analysis. II. Event-related synchronization in the gamma band. Brain 121 (Pt 12):2301-2315.

Crone NE, Miglioretti DL, Gordon B, Sieracki JM, Wilson MT, Uematsu S, Lesser RP (1998b) Functional mapping of human sensorimotor cortex with electrocorticographic spectral analysis. I. Alpha and beta event-related desynchronization. Brain 121 (Pt 12):2271-2299.

References

Crutcher MD, Russo GS, Ye S, Backus DA (2004) Target-, limb-, and context-dependent neural activity in the cingulate and supplementary motor areas of the monkey. Exp Brain Res 158:278-288.

Cunnington R, Windischberger C, Deecke L, Moser E (2002) The preparation and execution of self-initiated and externally-triggered movement: a study of event-related fMRI. Neuroimage 15:373-385.

d'Avella A, Bizzi E (2005) Shared and specific muscle synergies in natural motor behaviors. Proc Natl Acad Sci U S A 102:3076-3081.

d'Avella A, Saltiel P, Bizzi E (2003) Combinations of muscle synergies in the construction of a natural motor behavior. Nat Neurosci 6:300-308.

Dancause N (2006) Vicarious function of remote cortex following stroke: recent evidence from human and animal studies. Neuroscientist 12:489-499.

Deecke L, Lang W (1996) Generation of movement-related potentials and fields in the supplementary sensorimotor area and the primary motor area. Adv Neurol 70:127-146.

Deiber MP, Honda M, Ibanez V, Sadato N, Hallett M (1999) Mesial motor areas in self-initiated versus externally triggered movements examined with fMRI: effect of movement type and rate. J Neurophysiol 81:3065-3077.

Donchin O, Gribova A, Steinberg O, Bergman H, Vaadia E (1998) Primary motor cortex is involved in bimanual coordination. Nature 395:274-278.

Donoghue JP, Sanes JN, Hatsopoulos NG, Gaal G (1998) Neural discharge and local field potential oscillations in primate motor cortex during voluntary movements. J Neurophysiol 79:159-173.

Evarts EV (1968) Relation of pyramidal tract activity to force exerted during voluntary movement. J Neurophysiol 31:14-27.

Feige B, Aertsen A, Kristeva-Feige R (2000) Dynamic synchronization between multiple cortical motor areas and muscle activity in phasic voluntary movements. J Neurophysiol 84:2622-2629.

Freeman WJ, Skarda CA (1985) Spatial EEG patterns, non-linear dynamics and perception: the neo-Sherringtonian view. Brain Res 357:147-175.

Ganguly K, Secundo L, Ranade G, Orsborn A, Chang EF, Dimitrov DF, Wallis JD, Barbaro NM, Knight RT, Carmena JM (2009) Cortical representation of ipsilateral arm movements in monkey and man. J Neurosci 29:12948-12956.

Georgopoulos AP, Schwartz AB, Kettner RE (1986) Neuronal population coding of movement direction. Science 233:1416-1419.

Georgopoulos AP, Crutcher MD, Schwartz AB (1989) Cognitive spatial-motor processes. 3. Motor cortical prediction of movement direction during an instructed delay period. Exp Brain Res 75:183-194.

Georgopoulos AP, Kalaska JF, Caminiti R, Massey JT (1982) On the relations between the direction of two-dimensional arm movements and cell discharge in primate motor cortex. J Neurosci 2:1527-1537.

Gerloff C, Richard J, Hadley J, Schulman AE, Honda M, Hallett M (1998) Functional coupling and regional activation of human cortical motor areas during simple, internally paced and externally paced finger movements. Brain 121 (Pt 8):1513-1531.

Gerloff C, Bushara K, Sailer A, Wassermann EM, Chen R, Matsuoka T, Waldvogel D, Wittenberg GF, Ishii K, Cohen LG, Hallett M (2006) Multimodal imaging of brain reorganization in motor areas of the contralesional hemisphere of well recovered patients after capsular stroke. Brain 129:791-808.

Gowen E, Miall RC (2007) Differentiation between external and internal cuing: an fMRI study comparing tracing with drawing. Neuroimage 36:396-410.

Graziano M (2006) The organization of behavioral repertoire in motor cortex. Annu Rev Neurosci 29:105-134.

Graziano MS, Aflalo TN, Cooke DF (2005) Arm movements evoked by electrical stimulation in the motor cortex of monkeys. J Neurophysiol 94:4209-4223.

Habas C, Cabanis EA (2008) Neural correlates of simple unimanual discrete and continuous movements: a functional imaging study at 3 T. Neuroradiology 50:367-375.

Heldman DA, Wang W, Chan SS, Moran DW (2006) Local field potential spectral tuning in motor cortex during reaching. IEEE Trans Neural Syst Rehabil Eng 14:180-183.

Hochberg LR, Serruya MD, Friehs GM, Mukand JA, Saleh M, Caplan AH, Branner A, Chen D, Penn RD, Donoghue JP (2006) Neuronal ensemble control of prosthetic devices by a human with tetraplegia. Nature 442:164-171.

Hoshi E, Tanji J (2004) Differential roles of neuronal activity in the supplementary and presupplementary motor areas: from information retrieval to motor planning and execution. J Neurophysiol 92:3482-3499.

Hoshi E, Shima K, Tanji J (1998) Task-dependent selectivity of movement-related neuronal activity in the primate prefrontal cortex. J Neurophysiol 80:3392-3397.

Hummel FC, Cohen LG (2006) Non-invasive brain stimulation: a new strategy to improve neurorehabilitation after stroke? Lancet Neurol 5:708-712.

Humphrey DR, Schmidt EM, Thompson WD (1970) Predicting measures of motor performance from multiple cortical spike trains. Science 170:758-762.

References

Jahanshahi M, Jenkins IH, Brown RG, Marsden CD, Passingham RE, Brooks DJ (1995) Self-initiated versus externally triggered movements. I. An investigation using measurement of regional cerebral blood flow with PET and movement-related potentials in normal and Parkinson's disease subjects. Brain 118 (Pt 4):913-933.

Jones RD, Donaldson IM, Parkin PJ (1989) Impairment and recovery of ipsilateral sensory-motor function following unilateral cerebral infarction. Brain 112 (Pt 1):113-132.

Kakei S, Hoffman DS, Strick PL (1999) Muscle and movement representations in the primary motor cortex. Science 285:2136-2139.

Kakei S, Hoffman DS, Strick PL (2001) Direction of action is represented in the ventral premotor cortex. Nat Neurosci 4:1020-1025.

Kalaska JF, Hyde ML (1985) Area 4 and area 5: differences between the load direction-dependent discharge variability of cells during active postural fixation. Exp Brain Res 59:197-202.

Kalaska JF, Cohen DA, Hyde ML, Prud'homme M (1989) A comparison of movement direction-related versus load direction-related activity in primate motor cortex, using a two-dimensional reaching task. J Neurosci 9:2080-2102.

Kamitani Y, Tong F (2005) Decoding the visual and subjective contents of the human brain. Nat Neurosci 8:679-685.

Kamitani Y, Tong F (2006) Decoding seen and attended motion directions from activity in the human visual cortex. Curr Biol 16:1096-1102.

Kim KH, Kim SS, Kim SJ (2006) Superiority of nonlinear mapping in decoding multiple single-unit neuronal spike trains: a simulation study. J Neurosci Methods 150:202-211.

Kurtzer I, Scott SH (2007) A multi-level approach to understanding upper limb function. Prog Brain Res 165:347-362.

Leuthardt EC, Schalk G, Wolpaw JR, Ojemann JG, Moran DW (2004) A brain-computer interface using electrocorticographic signals in humans. J Neural Eng 1:63-71.

Leuthardt EC, Miller KJ, Schalk G, Rao RP, Ojemann JG (2006) Electrocorticography-based brain computer interface--the Seattle experience. IEEE Trans Neural Syst Rehabil Eng 14:194-198.

Li A, Yetkin FZ, Cox R, Haughton VM (1996) Ipsilateral hemisphere activation during motor and sensory tasks. AJNR Am J Neuroradiol 17:651-655.

Lotze M, Markert J, Sauseng P, Hoppe J, Plewnia C, Gerloff C (2006) The role of multiple contralesional motor areas for complex hand movements after internal capsular lesion. J Neurosci 26:6096-6102.

Matsunami K, Hamada I (1981) Characteristics of the ipsilateral movement-related neuron in the motor cortex of the monkey. Brain Res 204:29-42.

McFarland DJ, Krusienski DJ, Wolpaw JR (2006) Brain-computer interface signal processing at the Wadsworth Center: mu and sensorimotor beta rhythms. Prog Brain Res 159:411-419.

Mehring C, Rickert J, Vaadia E, Cardosa de Oliveira S, Aertsen A, Rotter S (2003) Inference of hand movements from local field potentials in monkey motor cortex. Nat Neurosci 6:1253-1254.

Miller KJ, Schalk G, Fetz EE, den Nijs M, Ojemann JG, Rao RP Cortical activity during motor execution, motor imagery, and imagery-based online feedback. Proc Natl Acad Sci U S A 107:4430-4435.

Miller KJ, Leuthardt EC, Schalk G, Rao RP, Anderson NR, Moran DW, Miller JW, Ojemann JG (2007) Spectral changes in cortical surface potentials during motor movement. J Neurosci 27:2424-2432.

Moran DW, Schwartz AB (1999) Motor cortical representation of speed and direction during reaching. J Neurophysiol 82:2676-2692.

Moritz CT, Perlmutter SI, Fetz EE (2008) Direct control of paralysed muscles by cortical neurons. Nature 456:639-642.

Morrow MM, Pohlmeyer EA, Miller LE (2009) Control of muscle synergies by cortical ensembles. Adv Exp Med Biol 629:179-199.

Mulliken GH, Musallam S, Andersen RA (2008) Decoding trajectories from posterior parietal cortex ensembles. J Neurosci 28:12913-12926.

Murthy VN, Fetz EE (1992) Coherent 25- to 35-Hz oscillations in the sensorimotor cortex of awake behaving monkeys. Proc Natl Acad Sci U S A 89:5670-5674.

Mussa-Ivaldi FA (1988) Do neurons in the motor cortex encode movement direction? An alternative hypothesis. Neurosci Lett 91:106-111.

Nicolelis MA, Dimitrov D, Carmena JM, Crist R, Lehew G, Kralik JD, Wise SP (2003) Chronic, multisite, multielectrode recordings in macaque monkeys. Proc Natl Acad Sci U S A 100:11041-11046.

Nir Y, Fisch L, Mukamel R, Gelbard-Sagiv H, Arieli A, Fried I, Malach R (2007) Coupling between neuronal firing rate, gamma LFP, and BOLD fMRI is related to interneuronal correlations. Curr Biol 17:1275-1285.

Oliveri M, Turriziani P, Carlesimo GA, Koch G, Tomaiuolo F, Panella M, Caltagirone C (2001) Parieto-frontal interactions in visual-object and visual-spatial working memory: evidence from transcranial magnetic stimulation. Cereb Cortex 11:606-618.

References

Padoa-Schioppa C, Li CS, Bizzi E (2004) Neuronal activity in the supplementary motor area of monkeys adapting to a new dynamic environment. J Neurophysiol 91:449-473.

Paninski L, Fellows MR, Hatsopoulos NG, Donoghue JP (2004a) Spatiotemporal tuning of motor cortical neurons for hand position and velocity. J Neurophysiol 91:515-532.

Paninski L, Shoham S, Fellows MR, Hatsopoulos NG, Donoghue JP (2004b) Superlinear population encoding of dynamic hand trajectory in primary motor cortex. J Neurosci 24:8551-8561.

Papa SM, Artieda J, Obeso JA (1991) Cortical activity preceding self-initiated and externally triggered voluntary movement. Mov Disord 6:217-224.

Pedersen JR, Johannsen P, Bak CK, Kofoed B, Saermark K, Gjedde A (1998) Origin of human motor readiness field linked to left middle frontal gyrus by MEG and PET. Neuroimage 8:214-220.

Pfurtscheller G, Neuper C, Kalcher J (1993) 40-Hz oscillations during motor behavior in man. Neurosci Lett 164:179-182.

Pfurtscheller G, Graimann B, Huggins JE, Levine SP, Schuh LA (2003) Spatiotemporal patterns of beta desynchronization and gamma synchronization in corticographic data during self-paced movement. Clin Neurophysiol 114:1226-1236.

Pistohl T, Ball T, Schulze-Bonhage A, Aertsen A, Mehring C (2008) Prediction of arm movement trajectories from ECoG-recordings in humans. J Neurosci Methods 167:105-114.

Pohlmeyer EA, Solla SA, Perreault EJ, Miller LE (2007) Prediction of upper limb muscle activity from motor cortical discharge during reaching. J Neural Eng 4:369-379.

Radhakrishnan SM, Baker SN, Jackson A (2008) Learning a novel myoelectric-controlled interface task. J Neurophysiol 100:2397-2408.

Rao SM, Binder JR, Bandettini PA, Hammeke TA, Yetkin FZ, Jesmanowicz A, Lisk LM, Morris GL, Mueller WM, Estkowski LD, et al. (1993) Functional magnetic resonance imaging of complex human movements. Neurology 43:2311-2318.

Ray S, Crone NE, Niebur E, Franaszczuk PJ, Hsiao SS (2008) Neural correlates of high-gamma oscillations (60-200 Hz) in macaque local field potentials and their potential implications in electrocorticography. J Neurosci 28:11526-11536.

Reina GA, Moran DW, Schwartz AB (2001) On the relationship between joint angular velocity and motor cortical discharge during reaching. J Neurophysiol 85:2576-2589.

Rickert J, Oliveira SC, Vaadia E, Aertsen A, Rotter S, Mehring C (2005) Encoding of movement direction in different frequency ranges of motor cortical local field potentials. J Neurosci 25:8815-8824.

Sanchez JC, Gunduz A, Carney PR, Principe JC (2008) Extraction and localization of mesoscopic motor control signals for human ECoG neuroprosthetics. J Neurosci Methods 167:63-81.

Sanes JN, Donoghue JP (1993) Oscillations in local field potentials of the primate motor cortex during voluntary movement. Proc Natl Acad Sci U S A 90:4470-4474.

Schalk G, Miller KJ, Anderson NR, Wilson JA, Smyth MD, Ojemann JG, Moran DW, Wolpaw JR, Leuthardt EC (2008) Two-dimensional movement control using electrocorticographic signals in humans. J Neural Eng 5:75-84.

Schalk G, Kubanek J, Miller KJ, Anderson NR, Leuthardt EC, Ojemann JG, Limbrick D, Moran D, Gerhardt LA, Wolpaw JR (2007) Decoding two-dimensional movement trajectories using electrocorticographic signals in humans. J Neural Eng 4:264-275.

Schoffelen JM, Oostenveld R, Fries P (2008) Imaging the human motor system's beta-band synchronization during isometric contraction. Neuroimage 41:437-447.

Schwartz AB (1994) Distributed motor processing in cerebral cortex. Curr Opin Neurobiol 4:840-846.

Scott SH (2000a) Population vectors and motor cortex: neural coding or epiphenomenon? Nat Neurosci 3:307-308.

Scott SH (2000b) Role of motor cortex in coordinating multi-joint movements: is it time for a new paradigm? Can J Physiol Pharmacol 78:923-933.

Scott SH (2000c) Reply to 'One motor cortex, two different views'. Nat Neurosci 3:964-965.

Serruya MD, Hatsopoulos NG, Paninski L, Fellows MR, Donoghue JP (2002) Instant neural control of a movement signal. Nature 416:141-142.

Shelton FN, Reding MJ (2001) Effect of lesion location on upper limb motor recovery after stroke. Stroke 32:107-112.

Sochurkova D, Rektor I, Jurak P, Stancak A (2006) Intracerebral recording of cortical activity related to self-paced voluntary movements: a Bereitschaftspotential and event-related desynchronization/synchronization. SEEG study. Exp Brain Res 173:637-649.

Stark E, Drori R, Abeles M (2009) Motor cortical activity related to movement kinematics exhibits local spatial organization. Cortex 45:418-431.

Taira M, Boline J, Smyrnis N, Georgopoulos AP, Ashe J (1996) On the relations between single cell activity in the motor cortex and the direction and magnitude of three-dimensional static isometric force. Exp Brain Res 109:367-376.

References

Tanji J, Okano K, Sato KC (1988) Neuronal activity in cortical motor areas related to ipsilateral, contralateral, and bilateral digit movements of the monkey. J Neurophysiol 60:325-343.

Taylor DM, Tillery SI, Schwartz AB (2002) Direct cortical control of 3D neuroprosthetic devices. Science 296:1829-1832.

Thut G, Hauert C, Viviani P, Morand S, Spinelli L, Blanke O, Landis T, Michel C (2000) Internally driven vs. externally cued movement selection: a study on the timing of brain activity. Brain Res Cogn Brain Res 9:261-269.

Todorov E (2000) Direct cortical control of muscle activation in voluntary arm movements: a model. Nat Neurosci 3:391-398.

Truccolo W, Friehs GM, Donoghue JP, Hochberg LR (2008) Primary motor cortex tuning to intended movement kinematics in humans with tetraplegia. J Neurosci 28:1163-1178.

Vaillancourt DE, Thulborn KR, Corcos DM (2003) Neural basis for the processes that underlie visually guided and internally guided force control in humans. J Neurophysiol 90:3330-3340.

van Donkelaar P, Stein JF, Passingham RE, Miall RC (1999) Neuronal activity in the primate motor thalamus during visually triggered and internally generated limb movements. J Neurophysiol 82:934-945.

Velliste M, Perel S, Spalding MC, Whitford AS, Schwartz AB (2008) Cortical control of a prosthetic arm for self-feeding. Nature 453:1098-1101.

Verstynen T, Diedrichsen J, Albert N, Aparicio P, Ivry RB (2005) Ipsilateral motor cortex activity during unimanual hand movements relates to task complexity. J Neurophysiol 93:1209-1222.

Voytek B, Secundo L, Bidet-Caulet A, Scabini D, Stiver SI, Gean AD, Manley GT, Knight RT (2009) Hemicraniectomy: A New Model for Human Electrophysiology with High Spatio-temporal Resolution. J Cogn Neurosci.

Waldert S, Pistohl T, Braun C, Ball T, Aertsen A, Mehring C (2009) A review on directional information in neural signals for brain-machine interfaces. J Physiol Paris 103:244-254.

Wallis JD, Anderson KC, Miller EK (2001) Single neurons in prefrontal cortex encode abstract rules. Nature 411:953-956.

Weilke F, Spiegel S, Boecker H, von Einsiedel HG, Conrad B, Schwaiger M, Erhard P (2001) Time-resolved fMRI of activation patterns in M1 and SMA during complex voluntary movement. J Neurophysiol 85:1858-1863.

Wessberg J, Nicolelis MA (2004) Optimizing a linear algorithm for real-time robotic control using chronic cortical ensemble recordings in monkeys. J Cogn Neurosci 16:1022-1035.

Wessberg J, Stambaugh CR, Kralik JD, Beck PD, Laubach M, Chapin JK, Kim J, Biggs SJ, Srinivasan MA, Nicolelis MA (2000) Real-time prediction of hand trajectory by ensembles of cortical neurons in primates. Nature 408:361-365.

Wisneski KJ, Anderson N, Schalk G, Smyth M, Moran D, Leuthardt EC (2008) Unique cortical physiology associated with ipsilateral hand movements and neuroprosthetic implications. Stroke 39:3351-3359.

Wolpaw JR, McFarland DJ (2004) Control of a two-dimensional movement signal by a noninvasive brain-computer interface in humans. Proc Natl Acad Sci U S A 101:17849-17854.

Wolpaw JR, Birbaumer N, McFarland DJ, Pfurtscheller G, Vaughan TM (2002) Brain-computer interfaces for communication and control. Clin Neurophysiol 113:767-791.

Wu W, Gao Y, Bienenstock E, Donoghue JP, Black MJ (2006) Bayesian population decoding of motor cortical activity using a Kalman filter. Neural Comput 18:80-118.

Yazawa S, Ikeda A, Kunieda T, Ohara S, Mima T, Nagamine T, Taki W, Kimura J, Hori T, Shibasaki H (2000) Human presupplementary motor area is active before voluntary movement: subdural recording of Bereitschaftspotential from medial frontal cortex. Exp Brain Res 131:165-177.